Forecasting Development

Forecasting Research Technical Report No. 352

Influence of Meteorology on Aircraft Sound Propagation

April 2001

P. Agnew

Met Office , Forecasting Development , Room R321, London Road , Bracknell , Berkshire ,RG12 2SZ,
United Kingdom

00/0486

Forecasting Research
Technical Report No. 352

Influence of Meteorology on Aircraft Sound Propagation

by

P. Agnew

April 2001

The Met Office
Forecasting Development
Room R321
London Road
Bracknell
RG12 2SZ
United Kingdom

Met Office , Forecasting Development , Room R321, London Road , Bracknell , Berkshire ,RG12 2SZ, United Kingdom

Influence of Meteorology on Aircraft Sound Propagation

P. Agnew

April 2001

Influence of Meteorology on Aircraft Sound Propagation

P. Agnew

Abstract

The effects of varying meteorological conditions on the noise exposure parameter L_{se} for aircraft ascending out of Heathrow airport have been estimated. A ray-based model of sound propagation has been employed which allows refraction effects due to windspeed and temperature gradients to be taken into account. It is found that the effects on L_{se} are frequently appreciable within the first 5km or so of the ascent. However at points under the flight path beyond this 5km boundary the effects of meteorology are negligible. Within the ~5km region, maximum amplifications of the order of 1-2dB and attenuations approaching –20dB may occur under extreme weather conditions, with more typical weather conditions giving rise to proportionately smaller effects. The maximum attenuations occur at points roughly adjacent to the take-off point whilst the maximum amplifications occur with a broader distribution over a region 2 – 3 km after take-off. The conditions giving rise to these variations in noise exposure levels are strong winds and higher lying temperature inversions.

Contents

1. Introduction

The environmental impact of air travel due to aircraft noise is considerable, causing disturbance to people living in the vicinity of airports and under flight paths. As a result there is interest in understanding the way in which sound propagates from airborne aircraft down to the ground. The atmosphere has long been known to have a strong influence on the process of sound propagation [1,2]. A number of different mechanisms are operative, including a) the refraction of sound waves due to variations in the speed of sound as a result of wind and temperature gradients; b) the scattering of sound due to turbulent wind flow and c) attenuation of sound due to varying amounts of water vapour in the atmosphere. As discussed later in this report, the second two items in this list are unable to result in any amplification of noise exposure. The present report therefore only considers the first item in this list. Estimates of the influence of wind and temperature gradients on noise exposure contours in the vicinity of Heathrow airport are presented, using meteorological data from a nearby observing station.

2. Modelling Sound Propagation

The fundamental problems associated with describing acoustic wave propagation were substantially solved by the time of Rayleigh's classic work [3] on the theory of sound. More recent work has concentrated on deriving efficient numerical methods of solving the wave equation, often in complex geometries. For the problem of sound propagation in an atmosphere having variable refractive index, several different levels of approximation are possible. The most accurate approach would involve a numerical solution of the 3D wave equation. Whilst rigorous, this approach is difficult to implement and computationally expensive. An alternative, which is often employed in problems of both atmospheric and underwater acoustic propagation, is referred to as the 'Parabolic Equation' (PE) method. In this method the elliptical wave equation in two dimensions is reduced to a parabolic form by neglecting the second spatial derivative of the wave field in the direction of propagation [4,5]. The resulting equation can be solved by a Fourier Transform method, known as the 'split-step'. Sound modelling based on a PE approach is able to account for all of the usual phenomena associated with wave propagation, including refraction, diffraction and reflection from surfaces. A drawback with the technique is that, in general, the PE is only useful within about ±15° of the direction of propagation. Thus the technique is valuable in problems of predominantly 'forward' propagation but less well suited to problems where propagation over a broad range of angles needs to be considered.

A different approach altogether is taken in the 'ray approximation'. Just as light propagation is well described by rays under certain conditions, so sound waves can be treated in a ray approximation. This is the method used in the present work to assess the effect of meteorology on sound propagation from aircraft. As in the optical case, the rays are taken to propagate in a direction normal to that of the wave front. The condition for validity of this approach is that the fractional change in the speed of sound should be small over distances of the order of one wavelength. For all realistic atmospheric gradients of wind speed and temperature and for audible frequencies (approximately 20Hz to 20kHz) this condition is satisfied. The ray model is not expected to give reliable results in the vicinity of noise shadows (where the sound rays are refracted such that they never reach the surface) because in these regions the wave character of the acoustic field plays a crucial role. Similarly, ray treatments of sound propagation are unable to account for any diffraction phenomena. However

since we are concerned here with sound travelling from airborne aircraft to the ground, there are no intervening objects to introduce diffraction effects and so this limitation is irrelevant in the present case. Simple reflection of sound off the ground can be modelled with ray methods, but this effect has not been included for two reasons: firstly, we are primarily interested in identifying meteorological effects occurring in the atmosphere and secondly, for aircraft well above the ground the primary propagation path is directly from the source to the observation point. This is clear on the basis of simple geometrical considerations. However we note that this need not be the case for a source close to the ground. Chessell has shown [6] that in this case an acoustic wave propagating along the surface plays an important role in determining the sound intensity at a ground-based observation point.

3. Ray Equations

In order to track the path of sound rays as they travel from an airborne aircraft down to the ground, it is necessary to derive the differential equations governing their motion. The 3D wave equation provides the starting point:

$$\nabla^2 p = \frac{1}{c^2(\underline{r})}\frac{\partial^2 p}{\partial t^2} \tag{1}$$

In this equation p is the excess acoustic pressure and c is the speed of sound at position vector $\underline{r}$. It is useful to introduce a refractive index function n defined as

$$n(\underline{r}) = \frac{c_0}{c(\underline{r})} \quad , \tag{2}$$

where c_0 is a reference speed of sound (in this work taken to be that at the surface). Under the assumption that c varies slowly with r, it is straightforward [7] to develop a solution to (1) known as the 'eikonal equation':

$$\frac{d(n\hat{\underline{s}})}{ds} = \nabla n \tag{3}$$

$s(\underline{r})$ is known as the 'eikonal'. It has dimensions of length and it is a direct extension of the concept of optical path length in geometrical optics. The eikonal equation is effectively an equation of motion for the rays. In order to integrate it all that is needed is the initial ray direction and the refractive index function. It can be put in a more useful form for calculations by substituting (2) into (3) and carrying out the differentiations explicitly. The result is a set of three differential equations for the direction cosines (α, β, γ) of the ray:

$$\frac{d\alpha}{ds} = \frac{-1}{c}\left[(1-\alpha^2)\left(\frac{\partial c}{\partial x}\right) - \alpha\beta\left(\frac{\partial c}{\partial y}\right) - \alpha\gamma\left(\frac{\partial c}{\partial z}\right)\right]$$

$$\frac{d\beta}{ds} = \frac{-1}{c}\left[(1-\beta^2)\left(\frac{\partial c}{\partial y}\right) - \gamma\beta\left(\frac{\partial c}{\partial z}\right) - \alpha\beta\left(\frac{\partial c}{\partial x}\right)\right]$$

$$\frac{d\gamma}{ds} = \frac{-1}{c}\left[(1-\gamma^2)\left(\frac{\partial c}{\partial z}\right) - \alpha\gamma\left(\frac{\partial c}{\partial x}\right) - \beta\gamma\left(\frac{\partial c}{\partial y}\right)\right] \quad . \tag{4}$$

In the approximation of a stratified atmosphere, variations in x and y are neglected, resulting in the simplified equations

$$\frac{d\alpha}{ds} = \frac{\alpha\gamma}{c}\left(\frac{\partial c}{\partial z}\right)$$

$$\frac{d\beta}{ds} = \frac{\gamma\beta}{c}\left(\frac{\partial c}{\partial z}\right)$$

$$\frac{d\gamma}{ds} = \frac{-(1-\gamma^2)}{c}\left(\frac{\partial c}{\partial z}\right) \quad . \tag{5}$$

These equations are sufficient to track the path of a ray from the source to the ground and are the ones used in the present work.

In order to estimate the sound intensity I on the ground it is necessary to relate this to the distribution of sound rays crossing unit area. In fact these two quantities are directly proportional to each other:

$$I = K\left(\frac{dN}{dA}\right) \quad , \tag{6}$$

where K is a constant and dN is the number of rays crossing the element of area dA. K and dN are chosen by requiring that the number of rays emitted each second by the source times the energy associated with each ray equals the source power. A simple approach would be to 'count' the number of rays reaching each element of area. However this approach requires a large number of rays to be tracked in order to obtain an accurate estimate. A clue to a more efficient approach is obtained by re-writing (6) in the form

$$I = \frac{K}{\left(\frac{dA}{dN}\right)} \quad . \tag{7}$$

This suggests that the intensity can be evaluated by determining the size of the area closest to each ray. This method is used in the present work. It is more efficient because it is largely independent of the number of rays used to represent unit power of the sound source and so fewer rays need be traced for a given level of accuracy.

4. Model Description

The core of the model, written in PVWave, is a subroutine which calculates the sound intensity (in dB) on the ground for a uniform sound source at a specified height above the ground. Referred to a standard spherical polar coordinate system, rays are emitted from the source in an azimuthal plane with a uniform angular separation in $\hat{\theta}$. A subsequent allowance is made for the fact that a uniform source emits with uniform intensity per unit *solid* angle. The intensity on the ground in this plane is calculated and the plane is then rotated azimuthally and the process repeated. The number of planes in the full 360° can be set within the program, depending on the angular resolution deemed appropriate. In between planes the intensity is obtained by performing a cubic spline linking values on the planes, until a full intensity map on the ground is created.

The code has been set up to calculate noise exposure contours on the ground over the path of a typical ascent from London Heathrow (LHR). Noise exposure contours are defined in a similar way to the normal decibel scale. However whereas the normal decibel scale relates to a ratio of sound intensities, the noise exposure relates to the time integral of the intensity, i.e. the sound *energy*, measured at the source. The definition employed is

$$L_{se}(\underline{r}) = 10\log\left[\frac{1}{E_0}\int_0^T I(t;\underline{r})dt\right] \quad , \tag{8}$$

where $I(t;r)$ is the intensity variation at position r and time t. The subscript on L refers to the fact that this is a noise exposure index for a *single event* of duration T. The reference energy E_0 is taken to be 10^{-12}J. The quantity inside square brackets represents the ratio of the total sound energy arriving at position $\underline{r}$ after time T, to an energy of 1pJ received at the point r. Since L_{se} still represents the logarithm of the ratio of two similar quantities it is natural to retain the decibel (dB) as its unit. It is common when describing sound levels in dB to weight the various frequencies involved in a manner which approximates to the frequency sensitivity of the human ear. The so-called 'A'-weighting scheme is usually selected for this purpose. Ray models are inherently frequency independent and so such a scheme would be inappropriate in the present work. However a simple correspondence may be obtained with the 'A'-weighting scheme by noting that a weight of unity is assigned to a frequency of 1kHz. Therefore the present L_{se} calculations may be viewed as being representative of a source emitting sound at this frequency. The range of human hearing extends from about 20Hz to 20kHz and so this frequency is representative of the central part of this spectrum.

In order to calculate L_{se} it is necessary to allow the source to move in a manner which mimics the aircraft ascent. The source is moved on a grid with 200m spacing and the sound distribution on the ground re-evaluated at each grid point. The grid extends to around 24km from the origin, which is taken to be the point at which the aircraft is 100m above the ground. In addition, the grid extends 2.5 km either side of the aircraft flight path. Details of a typical ascent profile for a medium-sized passenger jet aircraft were provided by the CAA [8] and are shown in Appendix 1, figure A1. The corresponding aircraft speed is also shown. The speed is required in order to evaluate the time spent in each grid box.

The basic operation of the code in the absence of meteorological effects was validated in a number of different ways. The simplest check of the core ray trajectory program involved comparing the calculation of the sound intensity on the ground for the case of a simple monopole source radiating according to an inverse square law intensity distribution. The calculation of noise exposure contours L_{se} was checked by evaluating this quantity for the case of a simple source moving at a uniform speed v and a constant height h across the ground. For observation points directly below the source the integral in (8) can be evaluated analytically:

$$\int_{-\infty}^{\infty} I(t)dt = \frac{S}{4hv} \quad , \tag{9}$$

where S is the source strength in Watts. In the present work this was taken to have the value 4π Watts, corresponding to 120dB at a distance of 1m. Off axis the integral can be evaluated numerically (again, in the absence of meteorological effects) and the values predicted by the computer model agree well with these calculations.

4.1. Incorporating Meteorological Data

The main meteorological input data into the computer model are vertical profiles of temperature, wind speed and wind direction. From these data, profiles of gradients are calculated using a simple forward difference scheme. The dependence of the speed of sound on temperature is taken to be

$$c_L = \left(\frac{\gamma RT}{\overline{M}} \right)^{1/2} \quad , \tag{10}$$

where $\overline{M}$ represents a mole-averaged, mean molecular mass for the atmosphere, such that

$$\frac{R}{\overline{M}} = 287 \, \mathrm{JK^{-1}Kg^{-1}mol} \quad .$$

The value of the speed of sound given by (10) is isotropic and is referred to as the local speed of sound, identified by the subscript L.

The effect of windspeed v_W on the speed of sound on is assumed to be of the form

$$c = c_L + v_W \cos\delta \quad , \tag{11}$$

where δ is the angle between the wind velocity vector and the direction of propagation of the ray. If the wind velocity vector and the ray have direction cosines $(\alpha', \beta', \gamma')$ and (α, β, γ) respectively then

$$\cos\delta = \alpha\alpha' + \beta\beta' + \gamma\gamma' \quad . \tag{12}$$

5. Results

In the following discussion of results the aim has been to illustrate the trend and magnitudes of typical effects, rather than to give a complete presentation of all the calculations which have performed for the many different possible combinations of parameters. We have chosen to illustrate the effects of meteorological profiles in the following way: a 'baseline' calculation is performed to evaluate the noise exposure profile assuming a still atmosphere at uniform temperature. The noise exposure contours for this 'no meteorology' case are shown in figure 1a. In figure 1b this same dataset is shown in the form of a surface plot of the L_{se} values. This baseline is then subtracted from further calculations, performed with atmospheric variations, in order to reveal the effect of meteorology. The advantage of this procedure is that the resulting ΔL_{se} values depend only on the meteorological effects and are independent of the source power.

5.1. Analytical Meteorological Profiles

Prior to investigating the effect of real wind and temperature profiles it is instructive to illustrate the effects of temperature gradients and wind profiles described by simple analytical expressions. Figures 2a and 2b shows the ΔL_{se} profile for a uniform temperature gradient equal to the dry adiabatic lapse rate, $-9.8\text{x}10^{-3}$ Km^{-1}. Since the temperature gradient only has a component in the z-direction the plot is symmetrical about the centre-line. The diverging effect on the sound rays of the decreasing speed of sound with height is manifested as a lowering of L_{se} compared to the 'no meteorology' case. The effect of a temperature inversion is illustrated in figures 3a and 3b. A temperature gradient equal in magnitude but opposite in sign to the dry adiabatic lapse rate was assumed to extend up to a height of 1km. This would represent an unusually large extent for an inversion of this magnitude, but is not unphysical. In this case the converging effect of the increase in temperature with altitude results in positive ΔL_{se} values, which again, are symmetrical about the path of the aircraft. The maximum magnitude of the ΔL_{se} values due to realistic temperature gradients are of the order of unity and occur either side of the aircraft close to the start of the flight path, resulting in a characteristic 'valley' shape.

In order to illustrate the effect of wind shear an analytical profile of the form

$$v = a \tanh\left(\frac{z}{w}\right) \quad , \tag{13}$$

was employed. In this expression v is the wind speed at altitude z; a and w are adjustable parameters. This function increases rapidly for small z and then asymptotically approaches a constant value of magnitude a at z values of approximately 2 to $3w$. Real wind profiles are perhaps better approximated by a logarithmic function which continues to increase slowly with altitude. However the hyperbolic tangent function has the advantage of offering a plateau, above which there is no ray refraction, thus giving the opportunity to assess effects as the rays cross the transition region. In figures 4a and 4b the results for the profile

$$v = 10 \tanh\left(\frac{z}{200}\right) \text{ ms}^{-1} \quad , \tag{14}$$

are shown. The wind was directed along the $-\hat{y}$ axis. The magnitude of the effect is clearly much greater than that of a temperature gradient and is asymmetrical. The amplification of noise exposure downwind and its attenuation upwind is clearly apparent. Once again, the greatest effects occur towards the start of the flight path.

5.2. Observational Meteorological Profiles

In order to assess the influence of meteorology on L_{se} we have taken the following approach. For each season (Spring, Summer etc.) an arbitrary two week period was selected. Two sets of radiosonde data, for 11am and 11pm ascents (henceforth referred to as daytime and night-time ascents) from the Herstmonceaux weather station, were extracted from the Met Office database (MetDB) for the period. These datasets were combined to give day and night-time seasonal averages which could subsequently be used as a reference point for comparison with atypical weather conditions. Simple averages were taken of temperature and wind speed. An average wind direction (permitted to vary with altitude) was deduced by separately averaging the *(u,v)* components of wind speed. Since the MetDB primarily reports altitude via a pressure measurement, the height coordinate was calculated by integrating the hydrostatic equation, taking the surface pressure and temperature variations with height into account. These seasonal average profiles are shown in Appendix 2. The figures show the mean variations of four quantities: the temperature, wind speed, wind direction calculated by averaging wind speed components and finally, the wind direction calculated by a simple averaging procedure. This final curve was not used in actual calculations but was included to act as a simple check on the more involved component averaging procedure adopted.

The meteorological profiles for Winter and Summer daytime ascents are shown in figures 5a and 6a, with the corresponding ΔL_{se} values shown in figures 5b,c and 6b,c. The most notable feature of these results, identified with the analytical profiles in the previous section, is the strong effect close to the start of the ascent, falling off very rapidly to give no discernible effect beyond about 5km. The maximum attenuations are around –13dB for Winter, compared to around –3dB for the Summer profile. This is a consequence of the higher mean wind speed for the Winter profile. These maximum attenuations occur at points roughly adjacent to the take-off point. The maximum amplifications are of the order of 1dB in both cases, occurring in the region 2 – 3 km after take-off.

The meteorological profiles and ΔL_{se} values for Winter and Summer night-time ascents are shown in figures 7a,b,c and 8a,b,c respectively. The lighter winds have resulted in less strong upwind attenuations in both cases. In addition, both sets of results show the 'valley' feature, characteristic of the temperature inversions apparent in the meteorological profiles. It is of interest to compare typical daytime and night-time results. In figures 9a,b the ΔL_{se} values obtained by subtracting the Summer daytime L_{se} trace from the night-time trace are shown. The symmetrical inversion characteristic dominates the trace although the maximum magnitude of the differences is only around 1dB. This illustrates a typical variation in the magnitude of noise exposure between day and night-time.

5.3. Extreme Weather Conditions

The above results have illustrated the behaviour of ΔL_{se} profiles under averaged weather conditions. In this section the behaviour under more extreme conditions is investigated. The aim was to attempt to identify those conditions under which the greatest amplifications of noise exposure might be expected. One whole year's worth of data (from 2000) representing radiosonde ascents from Herstmonceaux were extracted from the MetDB. This included both 11am and 11pm ascents. In addition, during the first half of the year some ascents were also made at 5am and 5pm. These data were also included in the analysis.

Experience with evaluating ray trajectories has shown that if the sound source is located above a temperature inversion, its focussing effect is relatively small. Under these conditions the inversion merely places an inflection in the ray trajectory. In order to achieve significant focussing the source should be located underneath the inversion. This observation suggests that the greatest amplifications of L_{se} due to temperature profiles will occur for high level inversions, for which the aircraft is underneath the inversion for a greater portion of its ascent. With this in mind, the data were searched for high level inversions. Figure 10a shows the meteorological profile for the highest inversion identified, which occurred on 1/6/00. The corresponding L_{se} contours and ΔL_{se} values are shown in figures 10b,c. Once again, the characteristic 'valley' feature associated with inversions is apparent and the amplifications are indeed rather larger (~2dB) than observed with seasonally averaged data. An interesting feature of this profile is the existence of two regions of attenuation, either side of the centre-line. This is a consequence of the way in which the wind changes direction rapidly at low altitude.

The effect of wind-induced sound refraction is generally stronger than that of temperature. It is actually gradients of wind speed which result in refraction, rather than a high wind speed itself. However if a high wind speed is reached over a comparable distance then this clearly implies a high wind speed gradient therefore the data were searched to locate the windiest days of the year. In figure 11a the meteorological profile for 12/12/00 is shown. Wind speeds of around 40ms^{-1} were reached at altitudes up to 3km. The L_{se} contours and ΔL_{se} values for this meteorological profile are shown in figures 11b,c. Strong attenuations, approaching −20 dB, are apparent and amplifications of around 2dB are produced in the downwind region. Again, the maximum attenuations occur at points roughly adjacent to the take-off point and the maximum amplifications are in the region 2 – 3 km after take-off.

Finally in this section, days with a maximum wind speed which occurs roughly ten times per year have been analysed. These were selected as an interesting case because they represent weather conditions which are not so extreme as to disrupt flight schedules but which might give exaggerated noise amplifications. A typical meteorological profile is shown in figure 12a, with corresponding L_{se} contours and ΔL_{se} values in figures 12b,c. For these conditions the attenuations reach a maximum of around −13dB and maximum amplifications between 1-2dB are observed.

6. Discussion

A number of general trends can be identified in the results presented. The most notable feature is that the ground noise exposure contours are only significantly

influenced by the meteorological profile within about 5km of the start of the ascent. In fact the maximum attenuations occur roughly adjacent to the take-off point whilst the maximum amplifications occur with a broader distribution over a region 2 – 3 km after take-off. This ~5km portion of the ascent path is where the L_{se} values have the greatest magnitude and so is naturally the place where the greatest deviations might also be expected. In this region the integral in equation (8) is dominated by contributions from the early part of the ascent and so any sound ray deflections here have a large effect on the L_{se} values. At positions further along on the ground under the flight path, important contributions to the L_{se} integral are made over a wider range of the flight path and there exists greater scope for the cancellation of amplification and attenuation effects.

For a given wind and temperature profile the calculated sound attenuations are invariably stronger than the amplifications. This is a consequence of the well-known noise shadowing effect, where in principle the sound level might drop to zero inside a shadowed region. It was pointed out in section 2 that ray-based sound models are unreliable in the vicinity of shadow regions and caustics and so the absolute values of L_{se} must be treated with caution in these regions. However the underlying imbalance between attenuation and amplification values appears well established. Sound energy is indeed conserved in the model but there is no requirement for any 'conservation of L_{se} values' here, with the sum of attenuations and amplifications equating to zero.

With regard to the magnitude of the ΔL_{se} variations, it is worth pointing out the following features. Firstly, the nature of L_{se} is to smooth out any meteorological effects on the amount of sound energy reaching a given location in two ways: a) by taking the logarithm of the energy and b) by integrating over the entire flight path. In order to emphasise the first point, table 1 shows ΔL_{se} values and the corresponding ratio of sound energy E_1/E_2 for two different profiles.

ΔL_{se}	E_1/E_2
0.1	1.023
0.5	1.12
1	1.26
2	1.58
5	3.16
8	6.31
10	10.0

Table 1. Variation in sound energy corresponding to ΔL_{se} values

It can be seen that ΔL_{se} values around unity actually correspond to appreciable energy differences.

With regard to (b) above, it is noted that L_{se} was introduced as a useful measure of noise index precisely because it is able to take into account the entire flight path. The previous measure used by the CAA was a 'Noise and Number Index' (NNI) [9]. This took account of a daily average number of aircraft movements and their maximum sound level, L_{max}. It was regarded as unsatisfactory because it fails to take into

account the disturbance offered by lower level aircraft noise. A calculation of L_{se} is significantly more complicated than that of L_{max} but offers a better representation of levels of noise disturbance.

6.1 Recommendations for Further Work

It would clearly be desirable to attempt to correlate the present calculations with measurements of noise exposure contours at Heathrow. A straightforward comparison would be difficult because experimental values around a busy airport would necessarily include contributions from different aircraft. In order to account for multiple aircraft the CAA utilise another measure, referred to as L_{eq}, which gives a suitably averaged noise exposure level over a 16 hour period. Given information regarding the frequency of aircraft ascents and a more realistic representation of engine sound intensity levels it should be possible to estimate this parameter in conjunction with calculated L_{se} values for the different aircraft ascents. By comparing the results with surface meteorological data from the airport it would be interesting to attempt a correlation.

The calculations performed in the present work have not taken into account the effect of sound scattering due to atmospheric turbulence. On particularly gusty days this is expected to significantly modify the pattern of sound propagation. Modelling sound propagation in a turbulent atmosphere would require a considerably more sophisticated approach. However on the basis of simple physical arguments it can be argued that turbulence would lead to greater levels of attenuation rather than any amplification. The nature of random scattering which arises in turbulent fluids is to re-distribute energy. The present calculations have also not included the attenuation of sound due to atmospheric absorption processes. In neglecting both of these effects these calculations can be viewed as giving an upper limit to the degree of amplification likely to be produced. Further work in this area would be useful in quantifying both of these effects.

With regard to the operational use of meteorology – dependent noise exposure profiles, it would be interesting to investigate the possibility of adjusting flight paths with a view to negating the effects of weather-induced shifts in the contour pattern. Finally, it is noted that the results presented in this report have concentrated exclusively on aircraft take-off noise profiles. It would be straightforward to perform a study of noise exposure profiles for aircraft coming in to land.

7. Summary

The propagation of sound from aircraft ascending out of Heathrow airport has been modelled using a ray-based propagation description. The effects of varying meteorological conditions on the noise exposure index L_{se} have been investigated. In the region ~5km from take-off, maximum amplifications of the order of 1-2dB and attenuations approaching –20dB are estimated. The maximum attenuations occur at points roughly adjacent to the take-off point whilst the maximum amplifications occur with a broader distribution over a region 2 – 3 km after take-off. The greater magnitude of attenuation compared to amplification can be understood on the basis of noise shadow effects. These values are estimated for the more extreme weather conditions. Seasonally-averaged meteorological profiles give rise to proportionately smaller effects. The meteorological conditions which give these variations in noise

exposure levels are strong winds and temperature inversions. At the boundary of the ~5km zone aircraft have typically achieved a height of around 500m, thus inversions extending up to this height and above would be expected to give the greatest noise enhancement on the ground. For aircraft flying above the inversion the effects due to it are likely to be negligible.

Acknowledgements

I would like to thank Mr. R.W. Lunnon for many useful suggestions during the course of this investigation. Dr. D. Monkman of the CAA kindly provided the information regarding aircraft ascent profiles.

References

[1] Delaney, M.E., 'Sound propagation in the atmosphere: a historical review', Acustica 38 (4) 201 (1977).

[2] Ingard, U., 'Acoustics' in Handbook of Physics, ed. E.U. Condon and H. Odinshaw, McGraw-Hill (1967).

[3] Rayleigh, J.W.S., 'The Theory of Sound', Dover Publications (1967).

[4] Kuperman, W.A., 'Propagation of sound in the ocean', in 'Encyclopedia of acoustics', ed. M.J. Crocker, John Wiley & Sons, Inc. (1997).

[5] Brekhovskikh, L. and Lysanov, Yu., 'Fundamentals of Ocean Acoustics', Springer-Verlag (1982).

[6] Chessell, C.I., 'Meteorological and ground effects on the propagation of aircraft noise close to the Earth's surface', J. Sound and Vibration 60 (2) 251 (1978).

[7] Elmore, W.C. and Heald, M.A. 'The Physics of Waves', Dover Publications (1988).

[8] Monkman, D., Personal communication 27/2/2001.

[9] Ollerhead, J.B., 'The CAA aircraft noise contour model: ANCON version 1', DORA Report 9120 (1992).

List of figure captions

Some comments regarding the figure captions are necessary. Both the contour maps and surface plots display the noise exposure levels at points within a grid ±3km wide by 25 km long. The ground-based axes of both plots are therefore in km, with the contours and the vertical axis of the surface plots indicating the dB level. The meteorology figures show three types of data: temperature, wind speed (ws) and wind direction (wd). These parameters are all given up to an altitude of 3000m, shown along the horizontal axis. For the vertical axes, temperatures are given in Kelvin, wind speeds are shown in metres per second and wind directions are expressed in degrees from North.

Figure 1a. Noise exposure contours for 'no meteorology' case
Figure 1b. Surface plot of ΔL_{se} values for 'no meteorology' case
Figure 2a. Noise exposure contours for adiabatic lapse rate only
Figure 2b. Surface plot of ΔL_{se} values for adiabatic lapse rate only
Figure 3a. Noise exposure contours for temperature inversion
Figure 3b. Surface plot of ΔL_{se} values for temperature inversion
Figure 4a. Noise exposure contours for analytical wind profile
Figure 4b. Surface plot of ΔL_{se} values for analytical wind profile
Figure 5a. Meteorological profile for averaged Winter daytime
Figure 5b. Noise exposure contours for averaged Winter daytime
Figure 5c. Surface plot of ΔL_{se} values for averaged Winter daytime
Figure 6a. Meteorological profile for averaged Summer daytime
Figure 6b. Noise exposure contours for averaged Summer daytime
Figure 6c. Surface plot of ΔL_{se} values for averaged Summer daytime
Figure 7a. Meteorological profile for averaged Winter nighttime
Figure 7b. Noise exposure contours for averaged Winter nighttime
Figure 7c. Surface plot of ΔL_{se} values for averaged Winter nighttime
Figure 8a. Meteorological profile for averaged Summer nighttime
Figure 8b. Noise exposure contours for averaged Summer nighttime
Figure 8c. Surface plot of ΔL_{se} values for averaged Summer nighttime
Figure 9a. Noise exposure contours for Summer daytime and nighttime
Figure 9b. Surface plot of ΔL_{se} values for Summer daytime and nighttime
Figure 10a. Meteorological profile for high level inversion
Figure 10b. Noise exposure contours for high level inversion
Figure 10c. Surface plot of ΔL_{se} values for high level inversion
Figure 11a. Meteorological profile for highest wind speed
Figure 11b. Noise exposure contours for highest wind speed
Figure 11c. Surface plot of ΔL_{se} values for highest wind speed
Figure 12a. Meteorological profile for wind speed occurring around ten times per year
Figure 12b. Noise exposure contours for wind speed occurring around ten times per year
Figure 12c. Surface plot of ΔL_{se} values for wind speed occurring around ten times per year

Figure A1. Height and speed variation used in noise calculations [8].

Figure A2a. Meteorological profile for averaged Winter daytime
Figure A2b. Meteorological profile for averaged Spring daytime
Figure A2c. Meteorological profile for averaged Summer daytime
Figure A2d. Meteorological profile for averaged Autumn daytime

Figure A3a. Meteorological profile for averaged Winter nighttime
Figure A3b. Meteorological profile for averaged Spring nighttime
Figure A3c. Meteorological profile for averaged Summer nighttime
Figure A3d. Meteorological profile for averaged Autumn nighttime

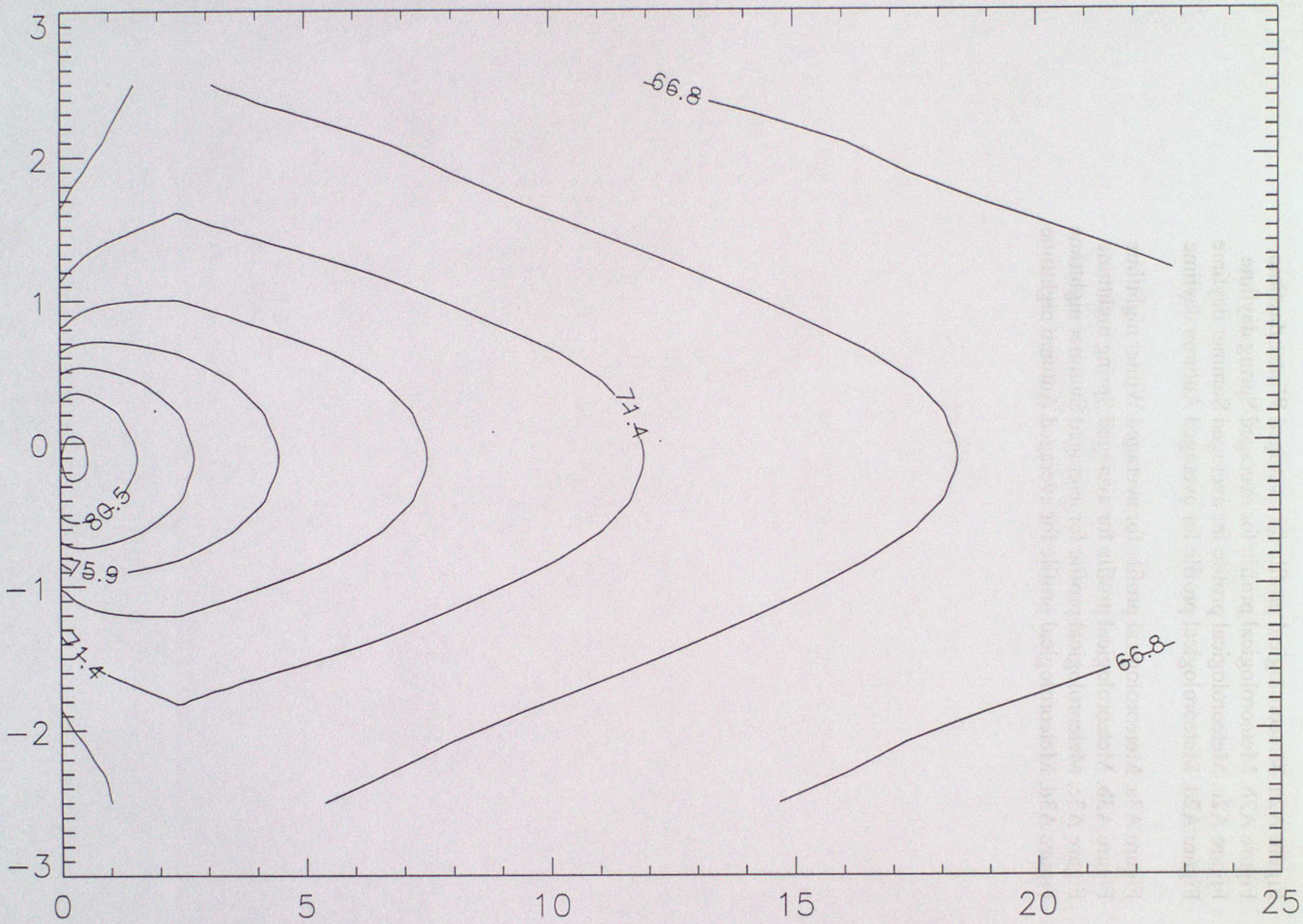

Figure 1a. Noise exposure contours for 'no meteorology' case

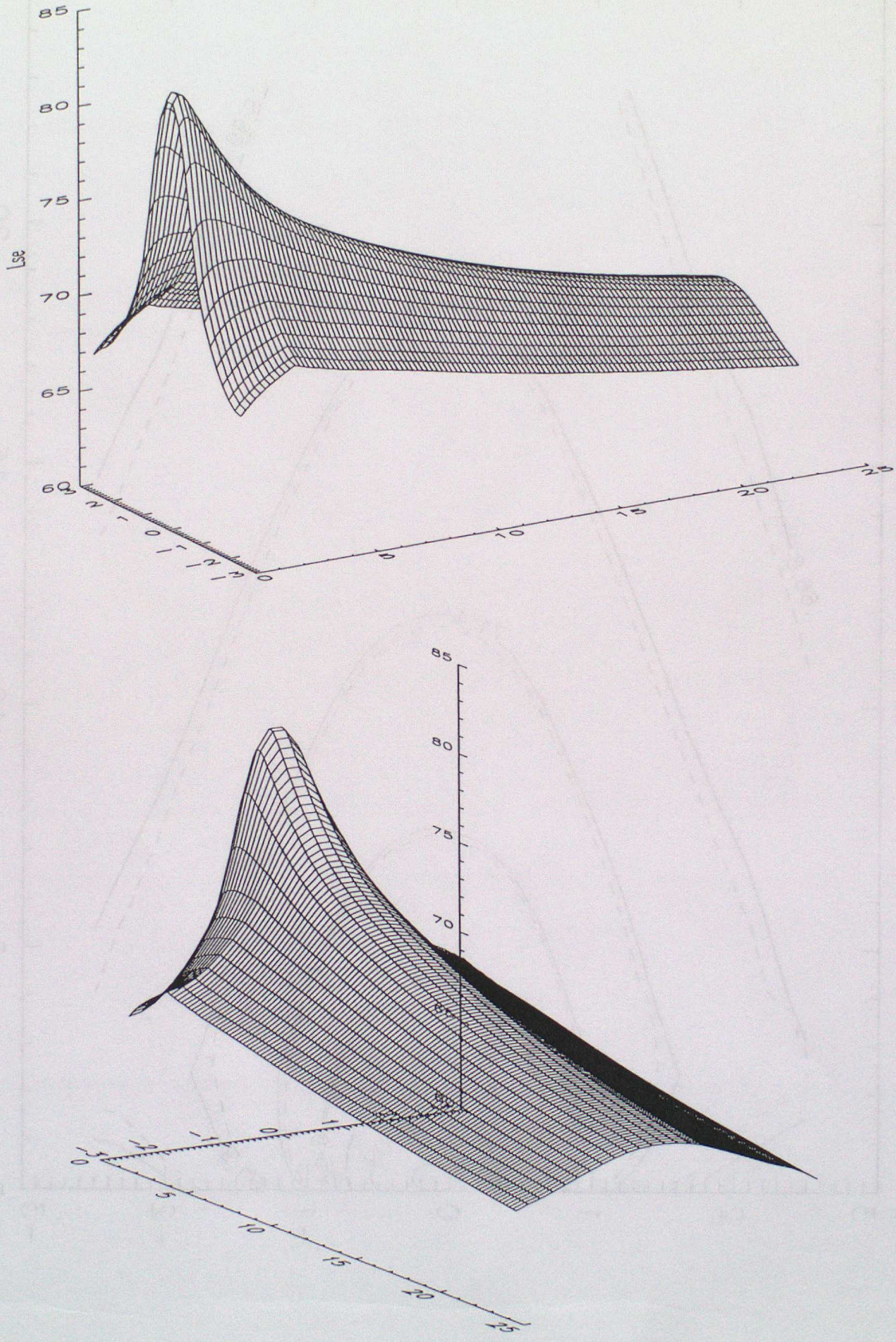

Figure 1b. Surface plot of ΔL_{se} values for 'no meteorology' case

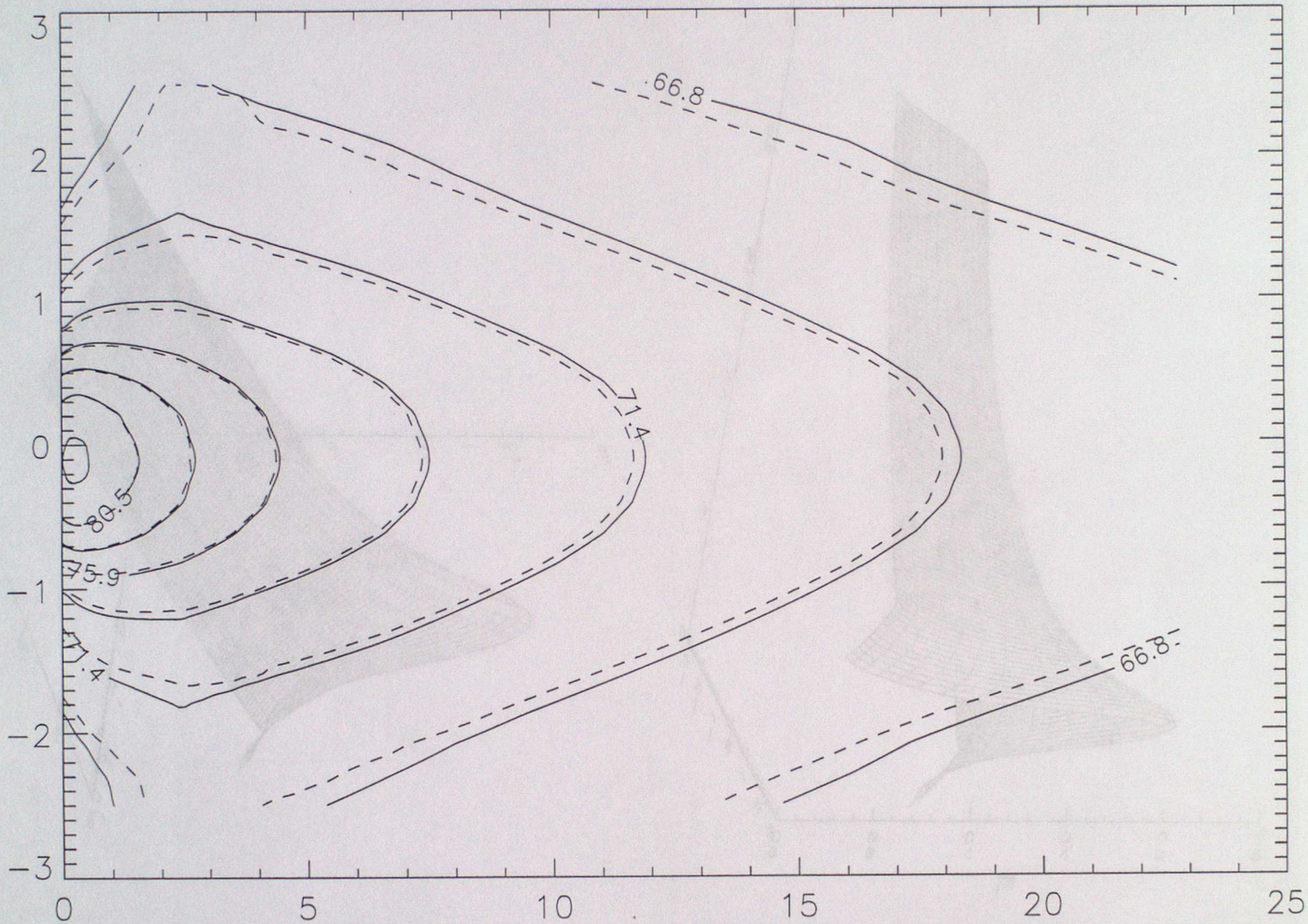

Figure 2a. Noise exposure contours for adiabatic lapse rate only

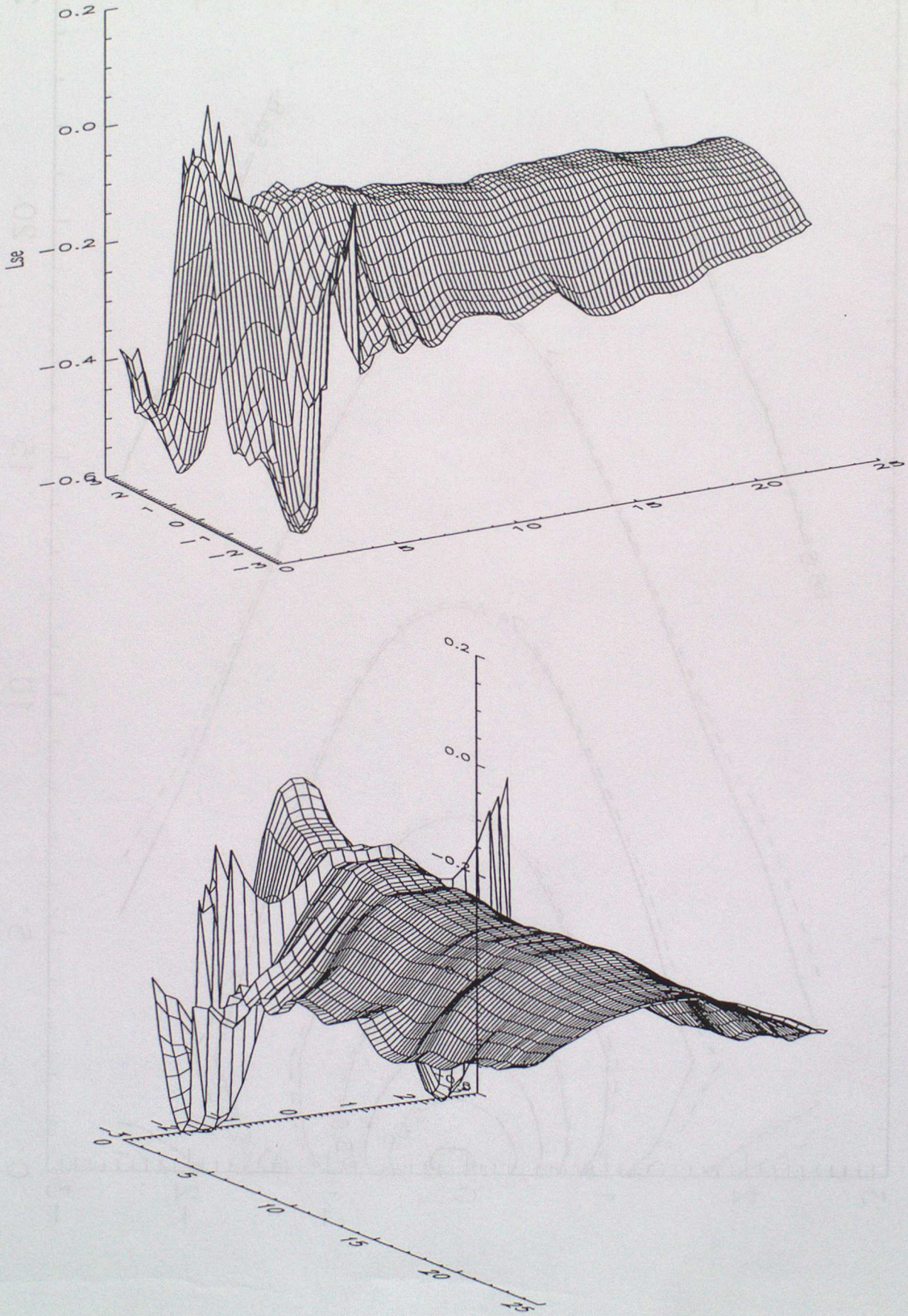

Figure 2b. Surface plot of ΔL_{se} values for adiabatic lapse rate only

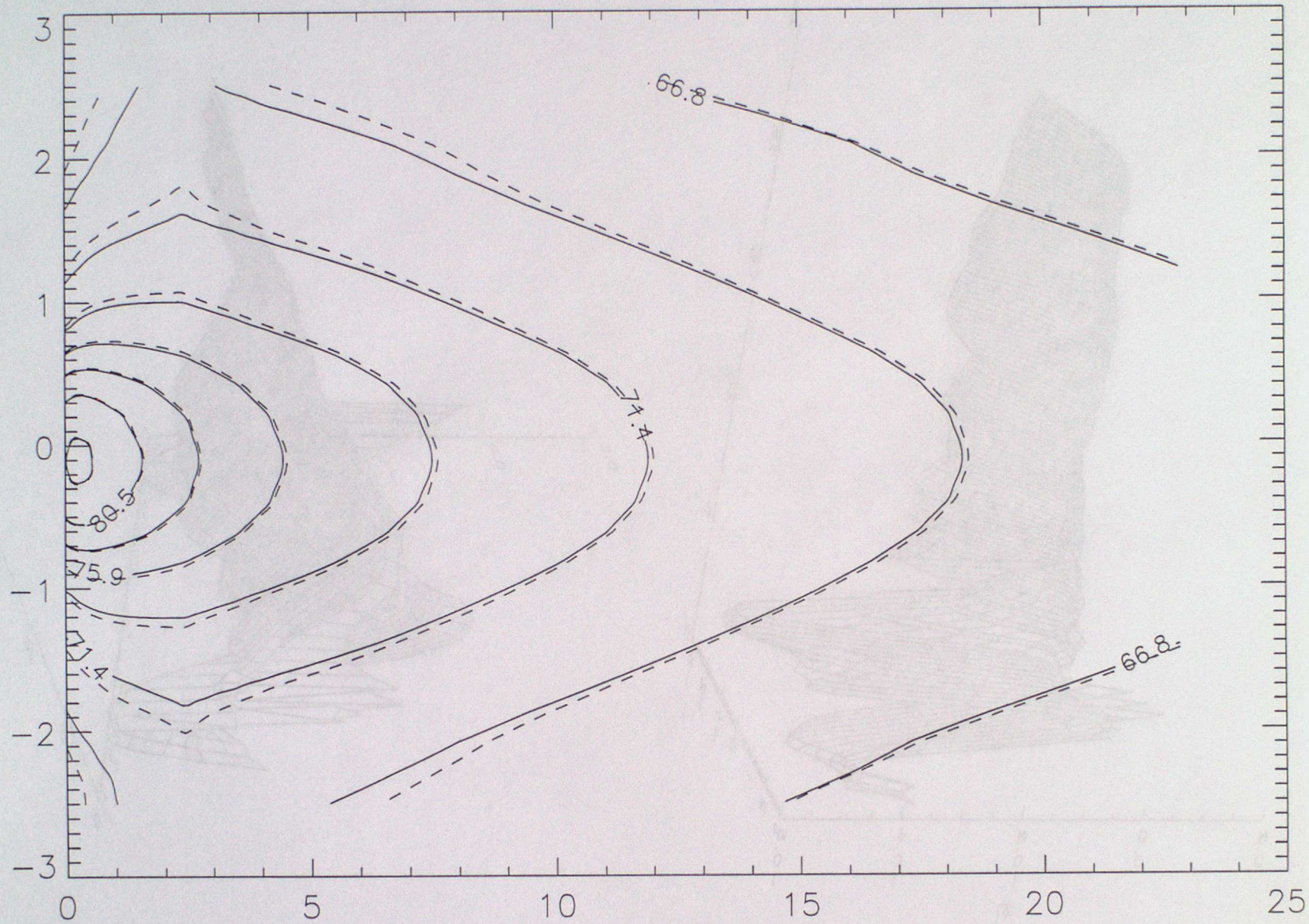

Figure 3a. Noise exposure contours for temperature inversion

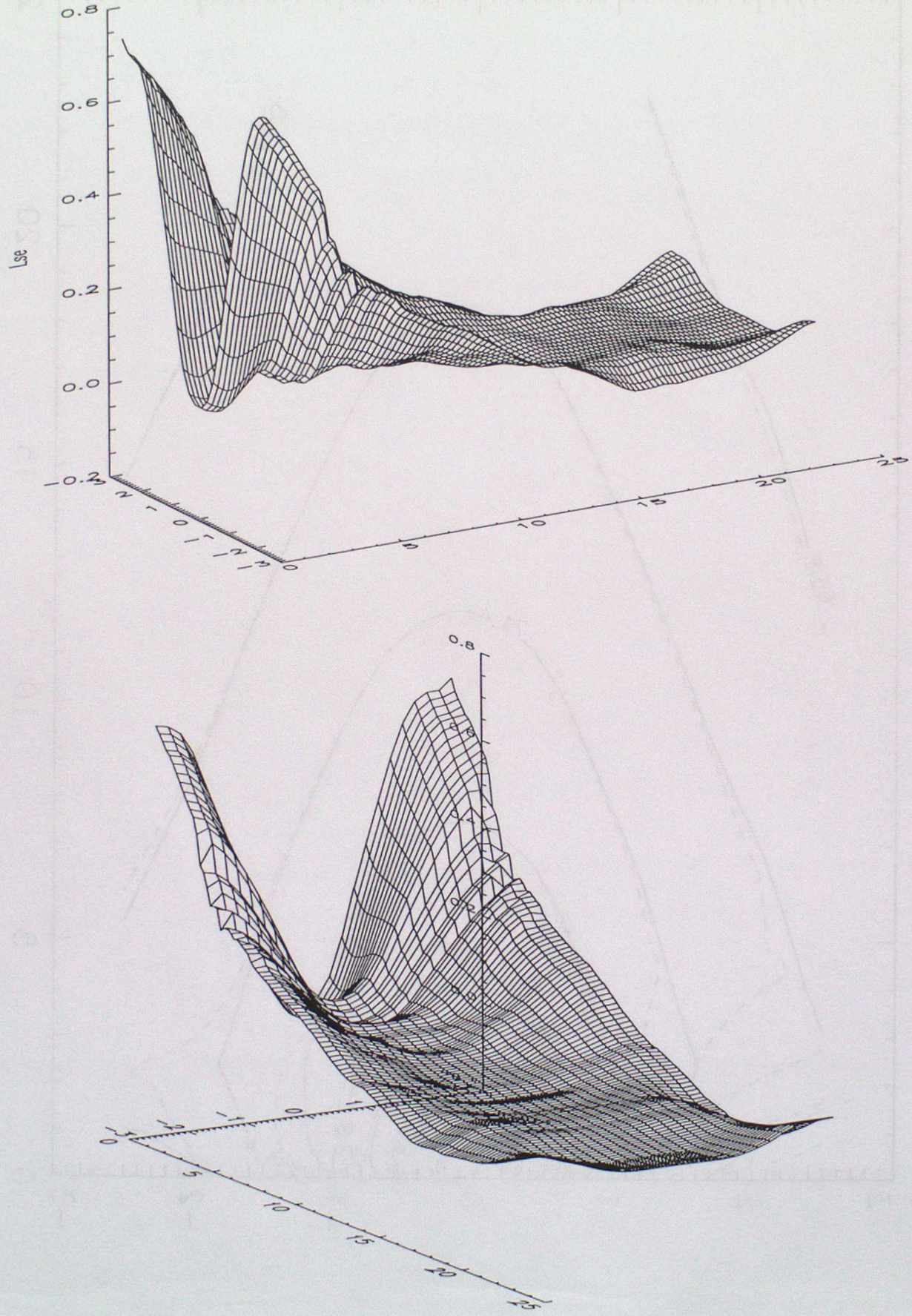

Figure 3b. Surface plot of ΔL_{se} values for temperature inversion

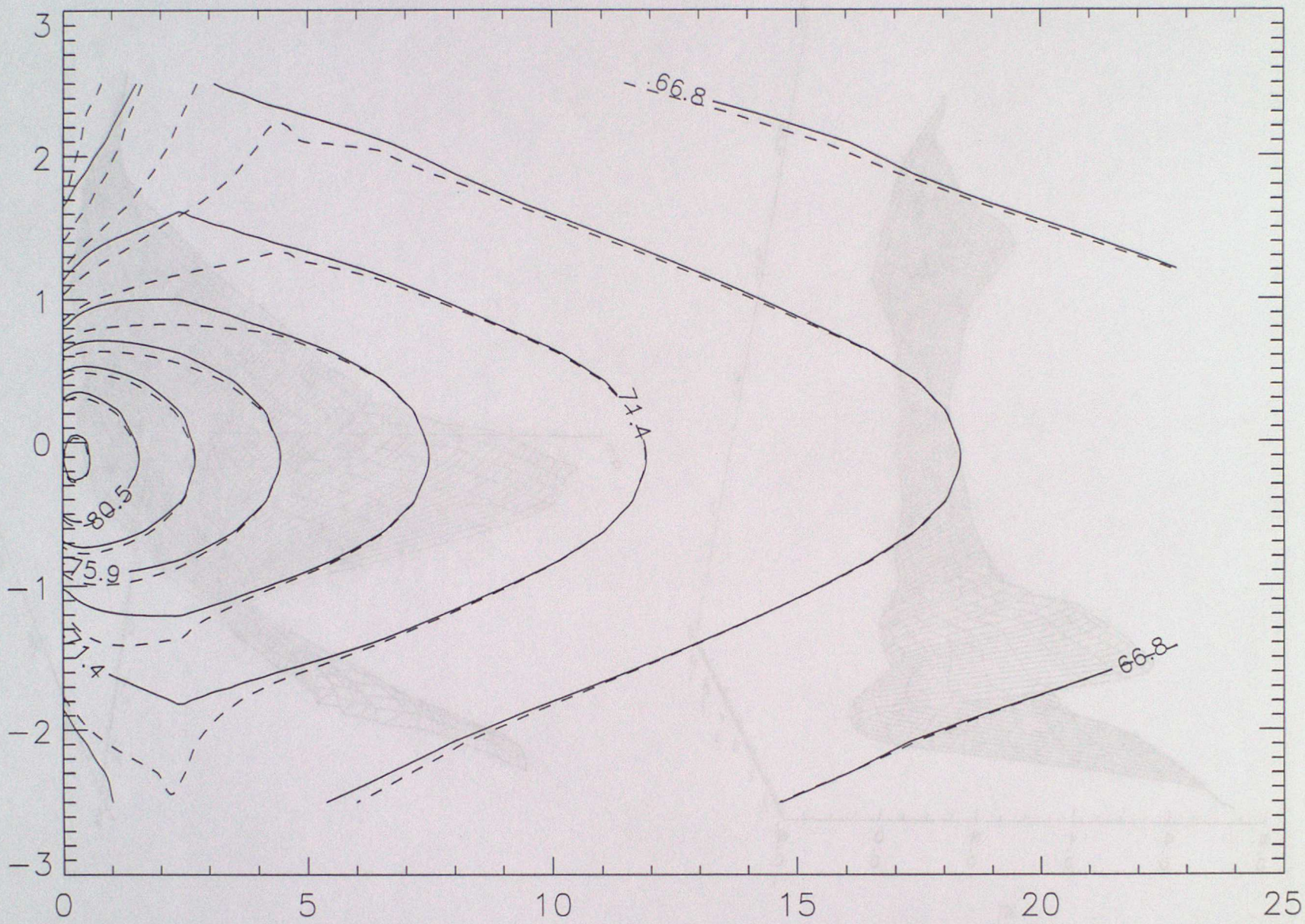

Figure 4a. Noise exposure contours for analytical wind profile

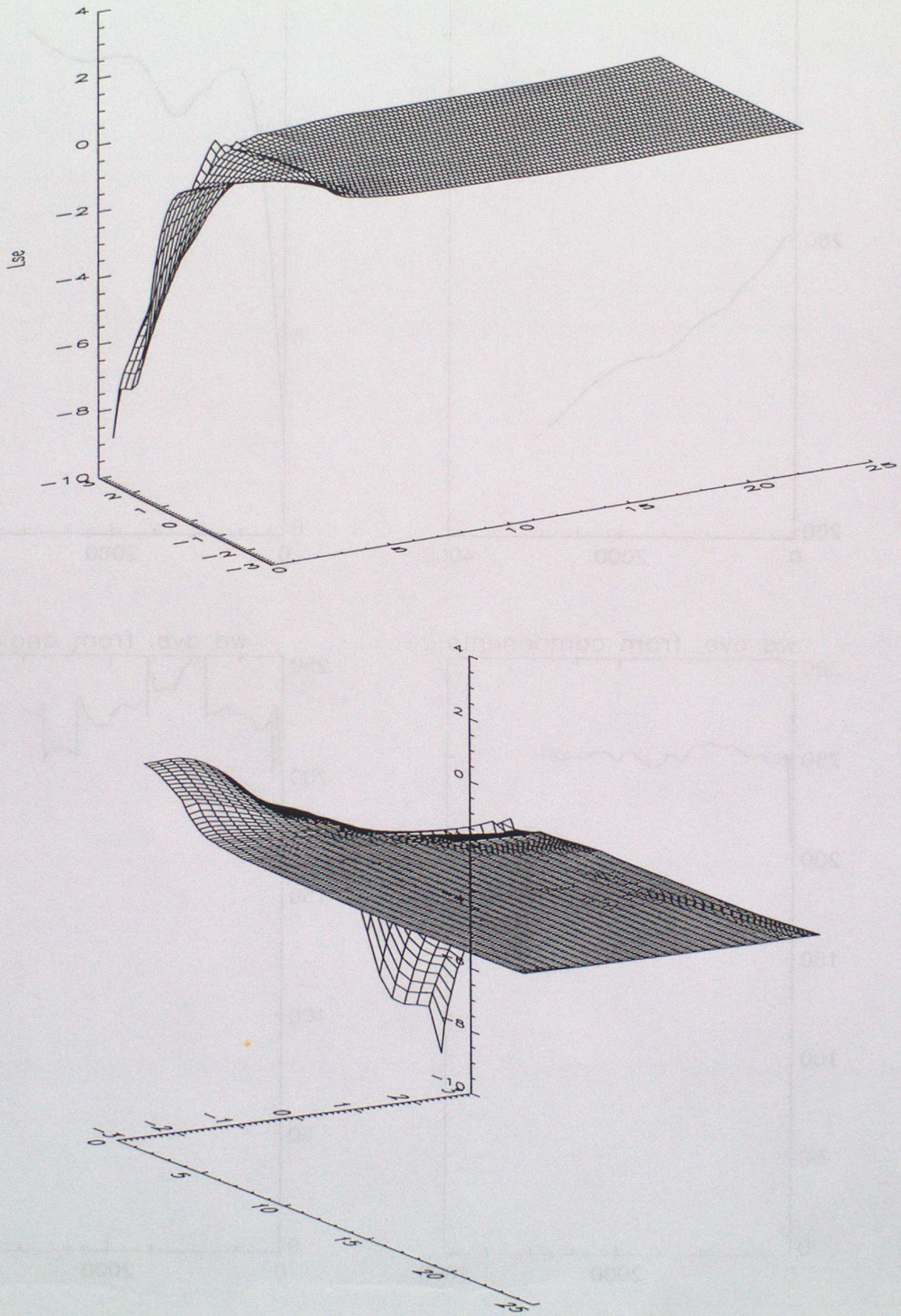

Figure 4b. Surface plot of ΔL_{se} values for analytical wind profile

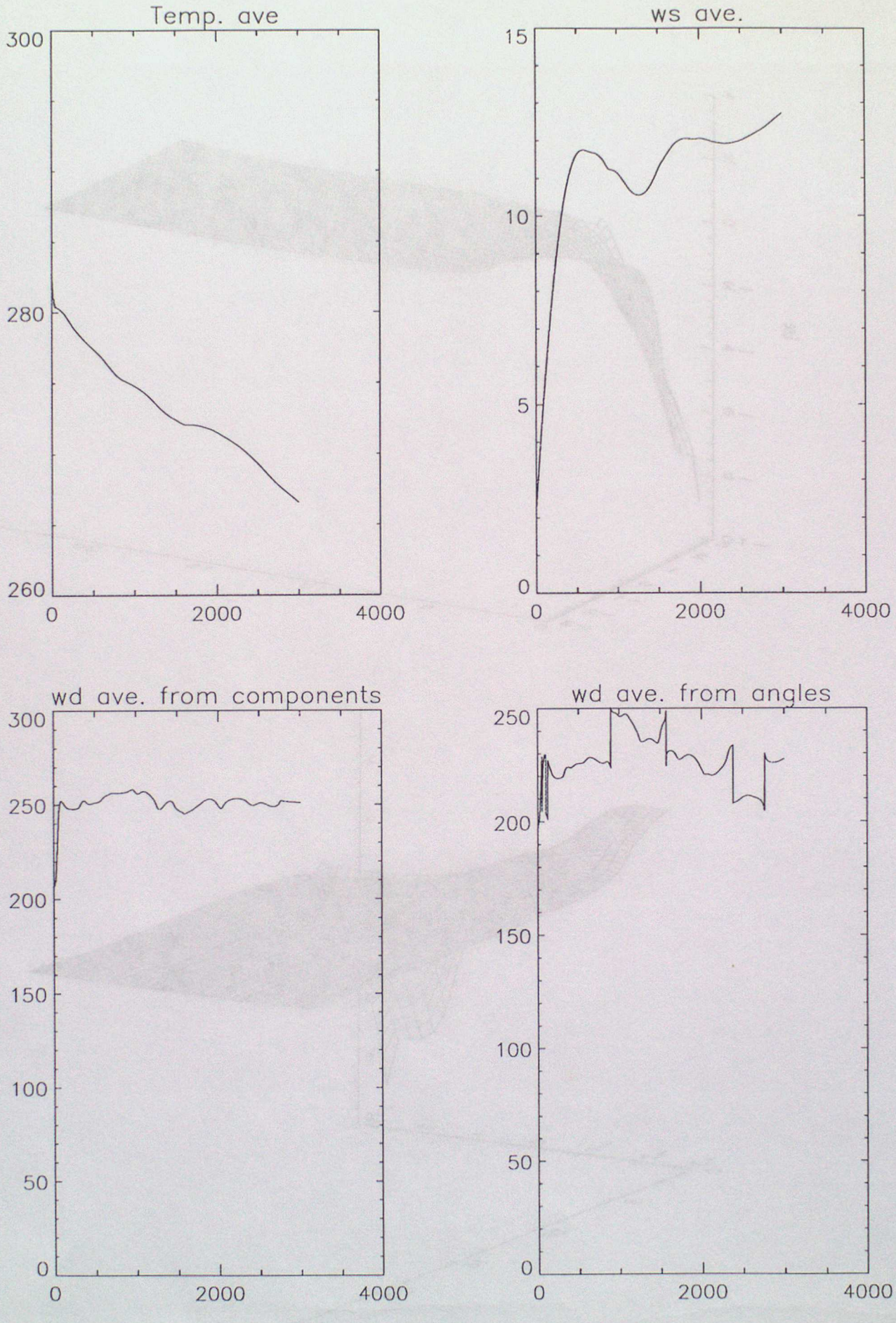

Figure 5a. Meteorological profile for averaged Winter daytime

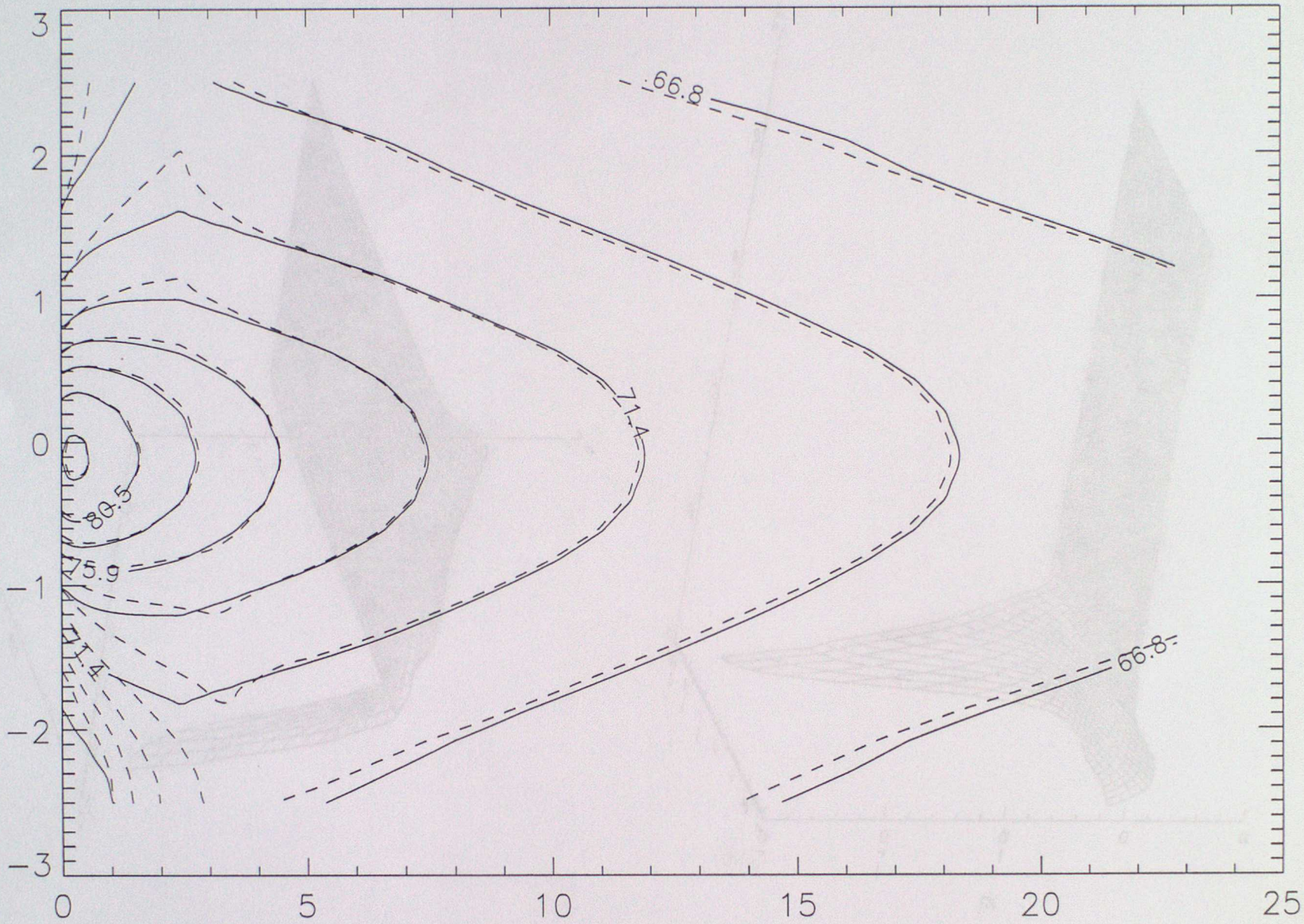

Figure 5b. Noise exposure contours for averaged Winter daytime

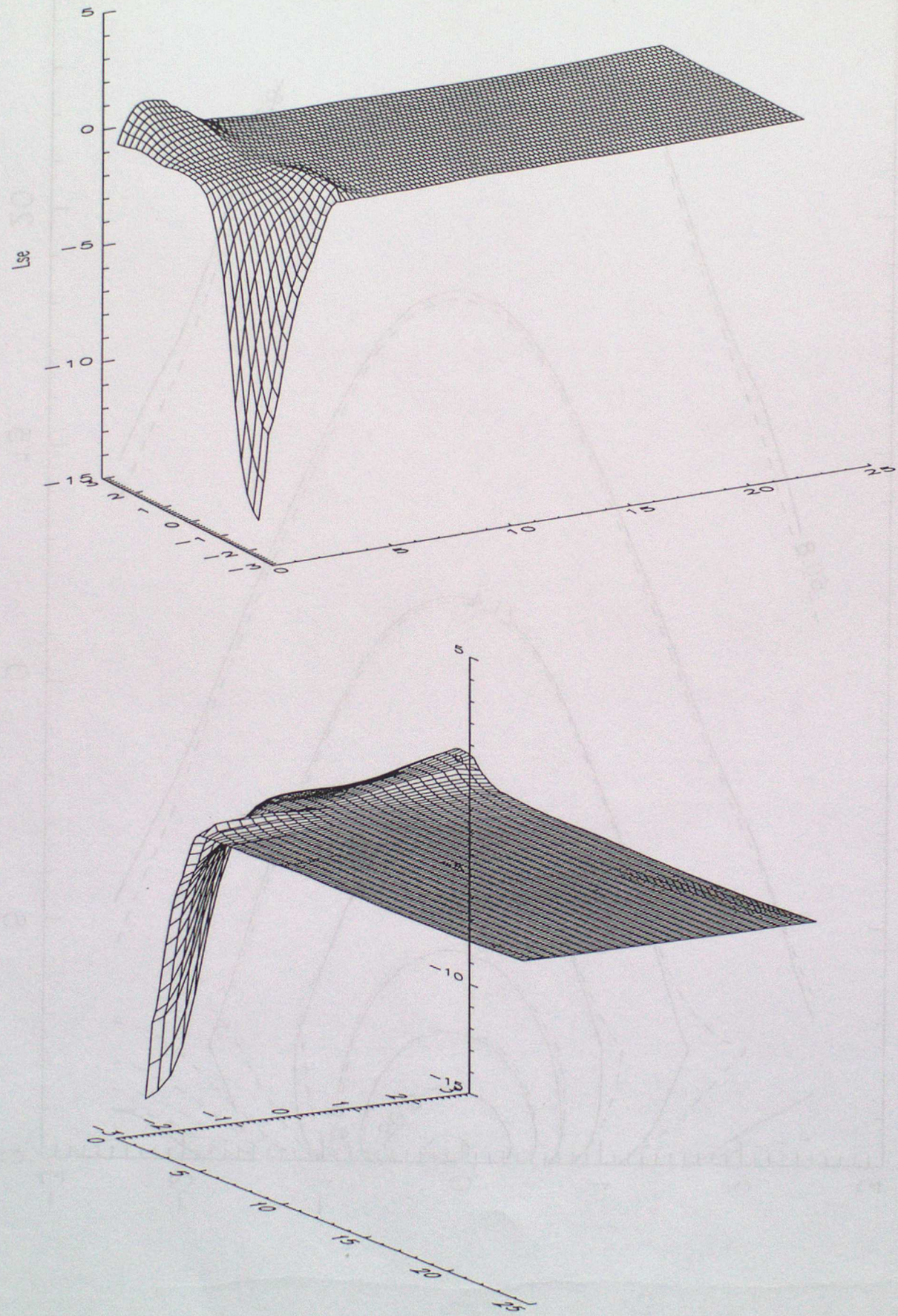

Figure 5c. Surface plot of ΔL_{se} values for averaged Winter daytime

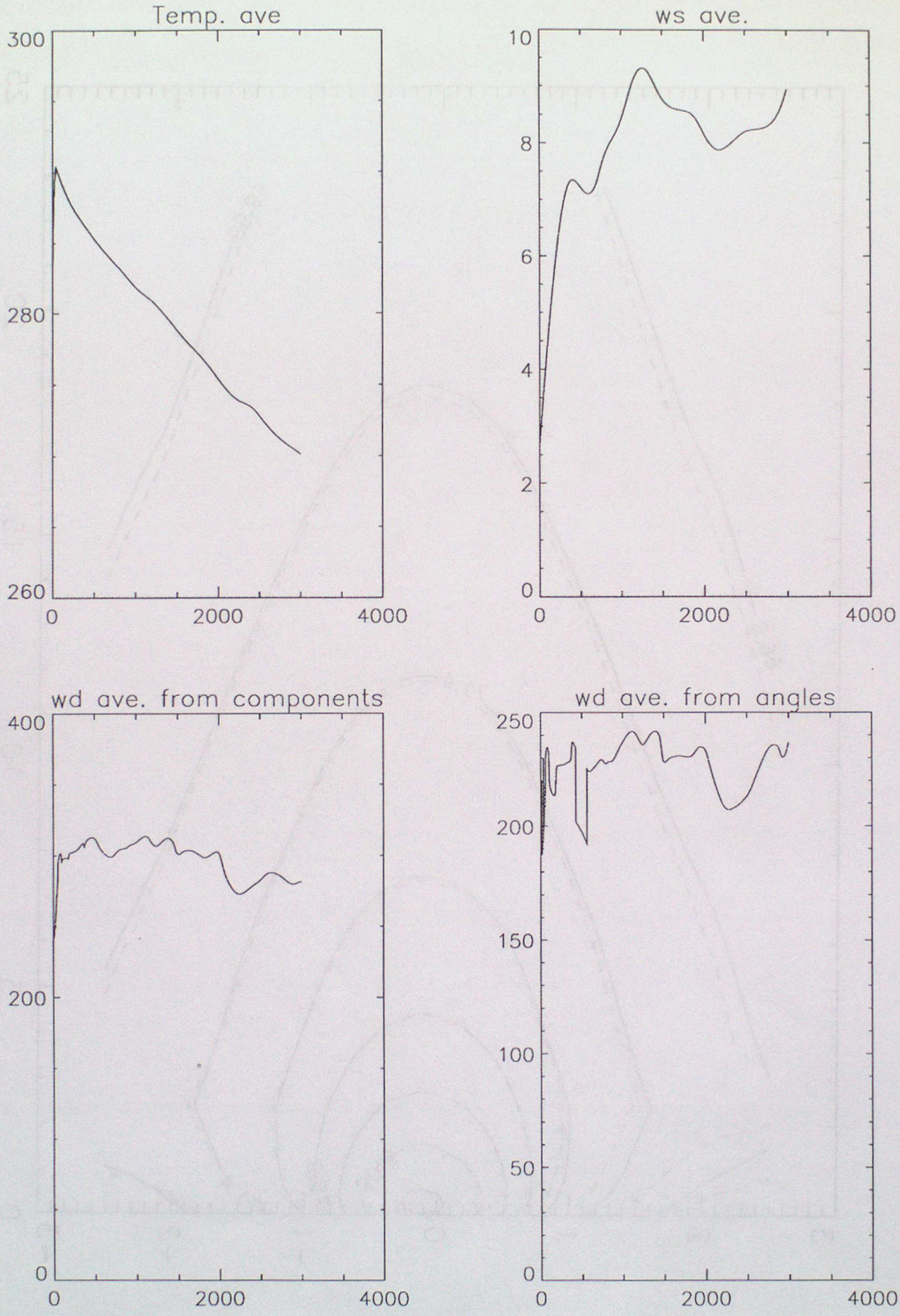

Figure 6a. Meteorological profile for averaged Summer daytime

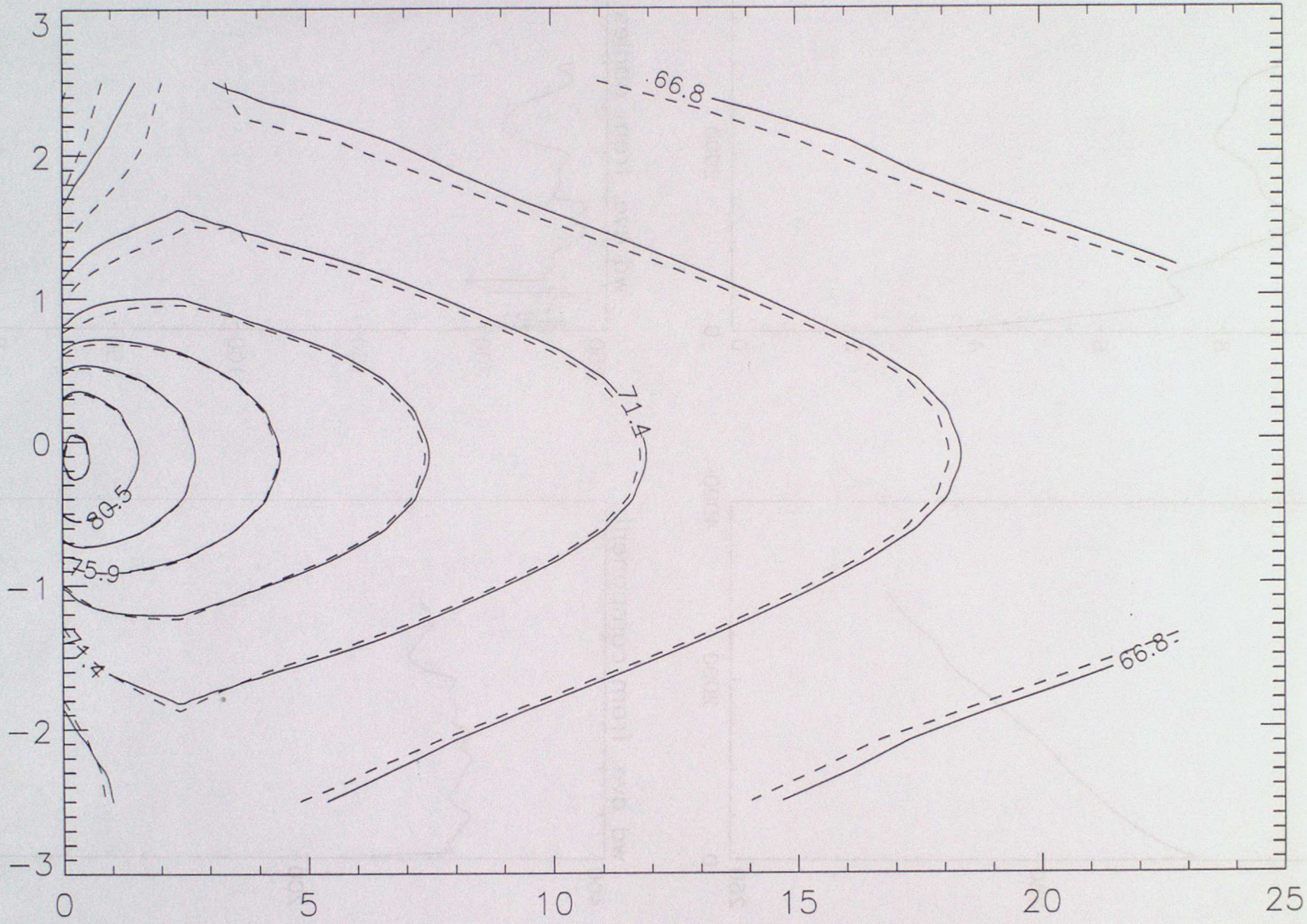

Figure 6b. Noise exposure contours for averaged Summer daytime

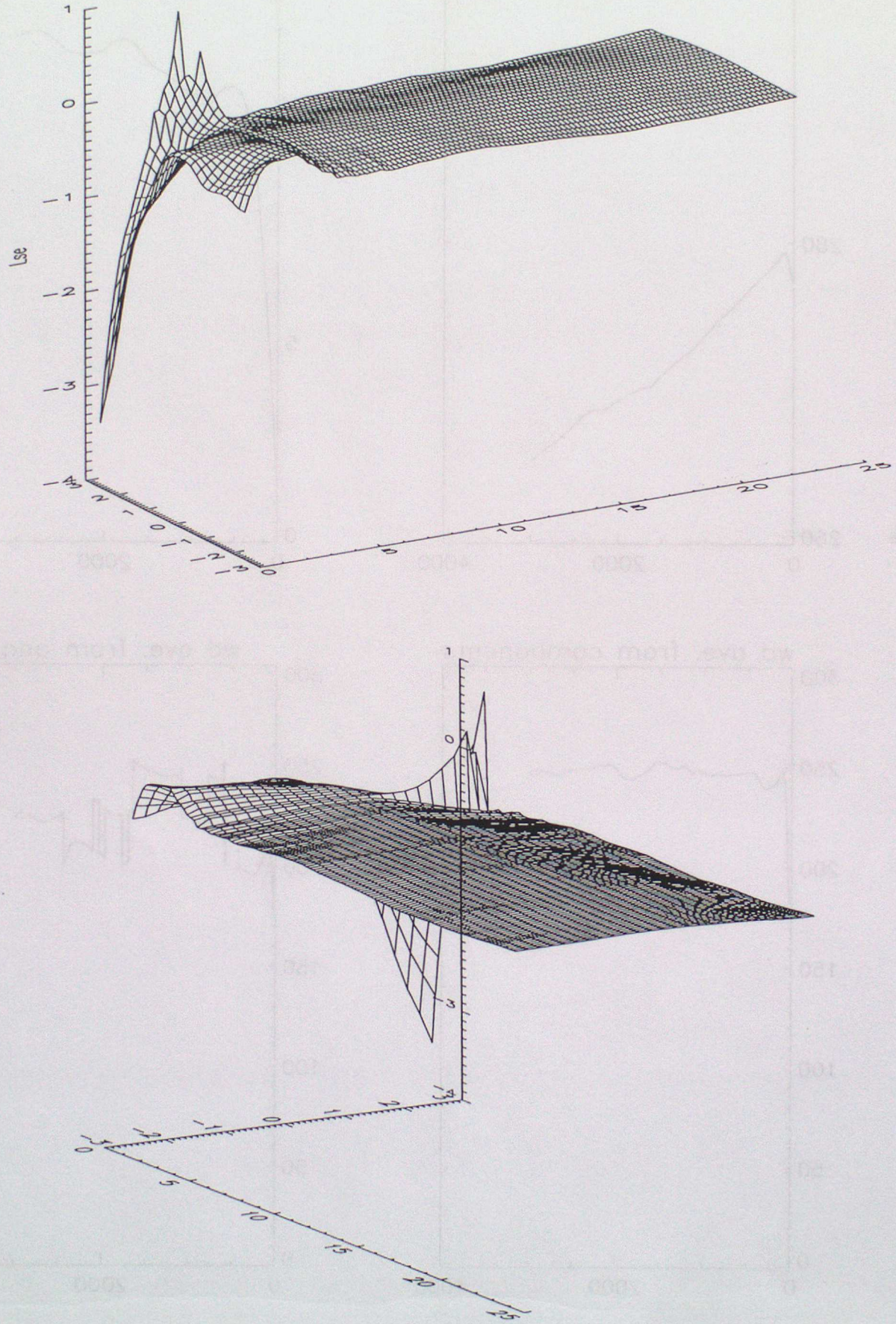

Figure 6c. Surface plot of ΔL_{se} values for averaged Summer daytime

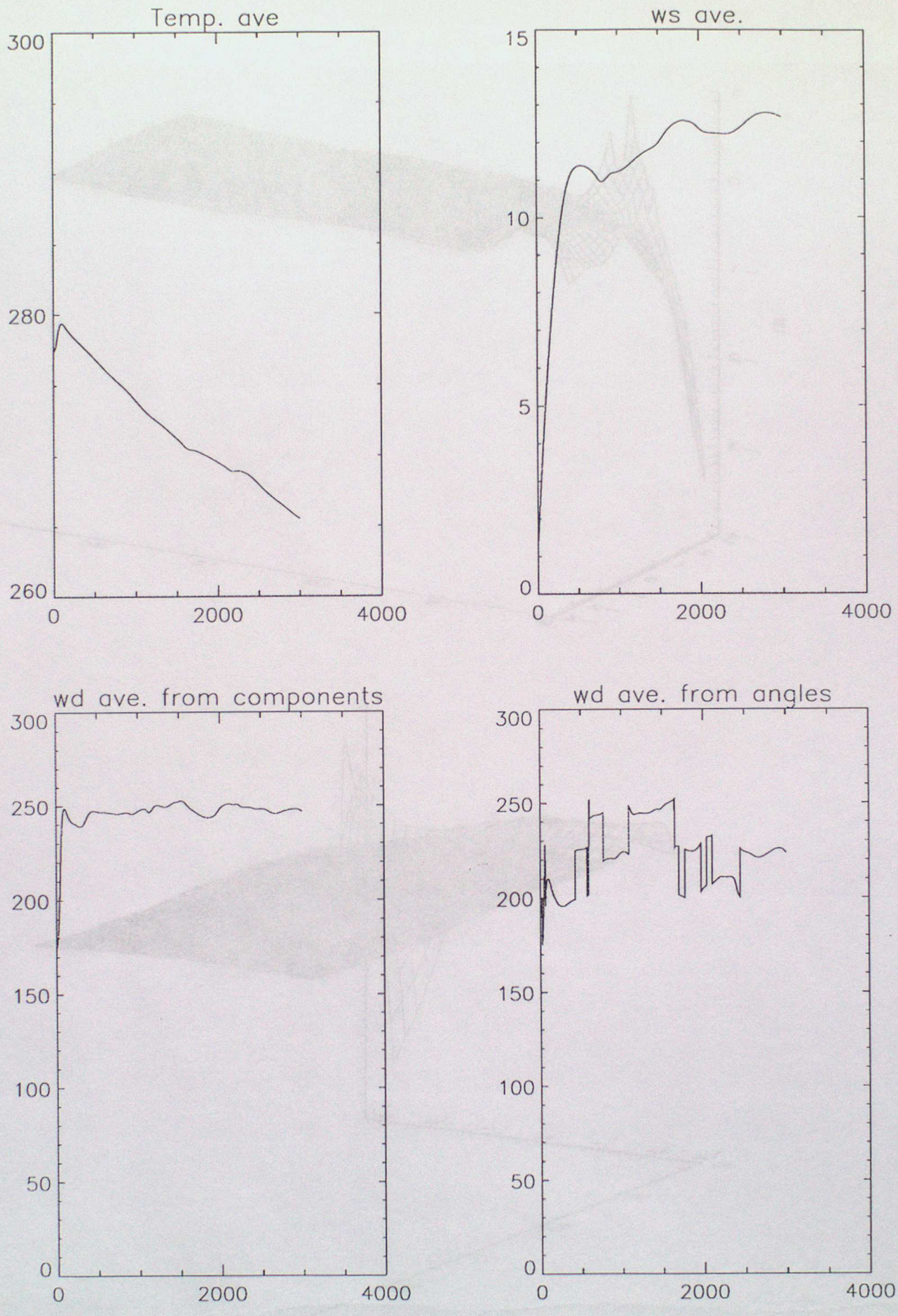

Figure 7a. Meteorological profile for averaged Winter nighttime

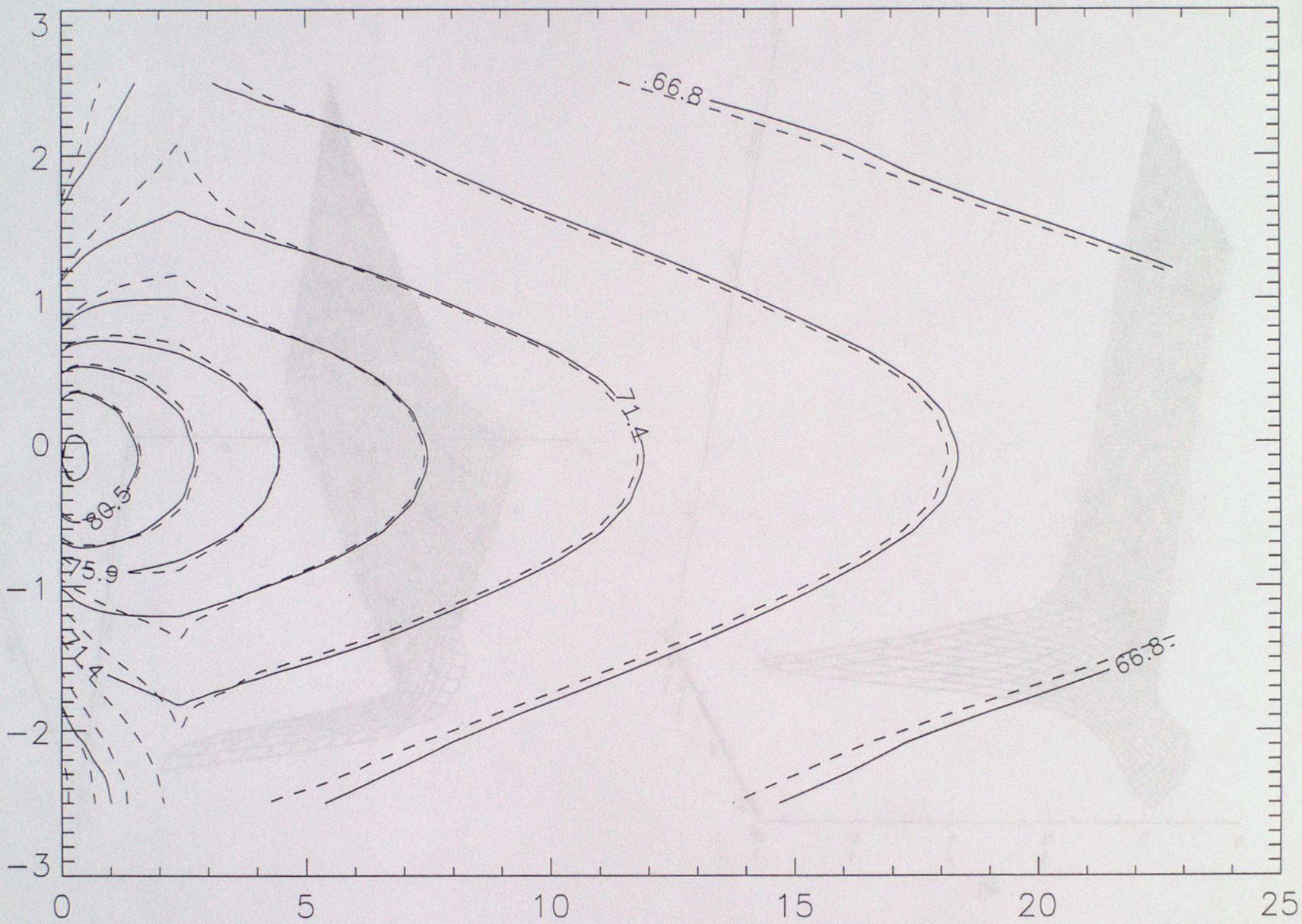

Figure 7b. Noise exposure contours for averaged Winter nighttime

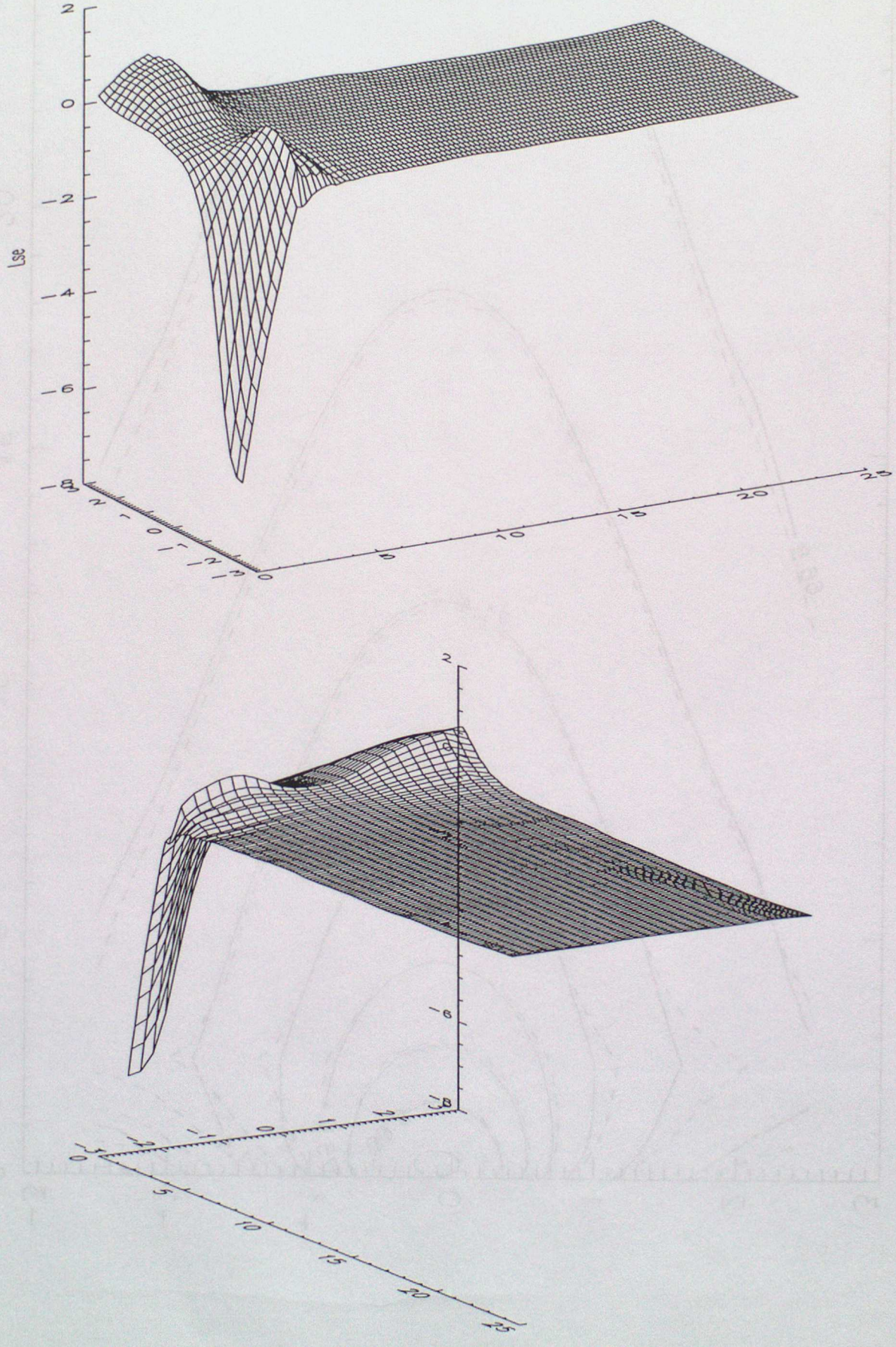

Figure 7c. Surface plot of ΔL_{se} values for averaged Winter nighttime

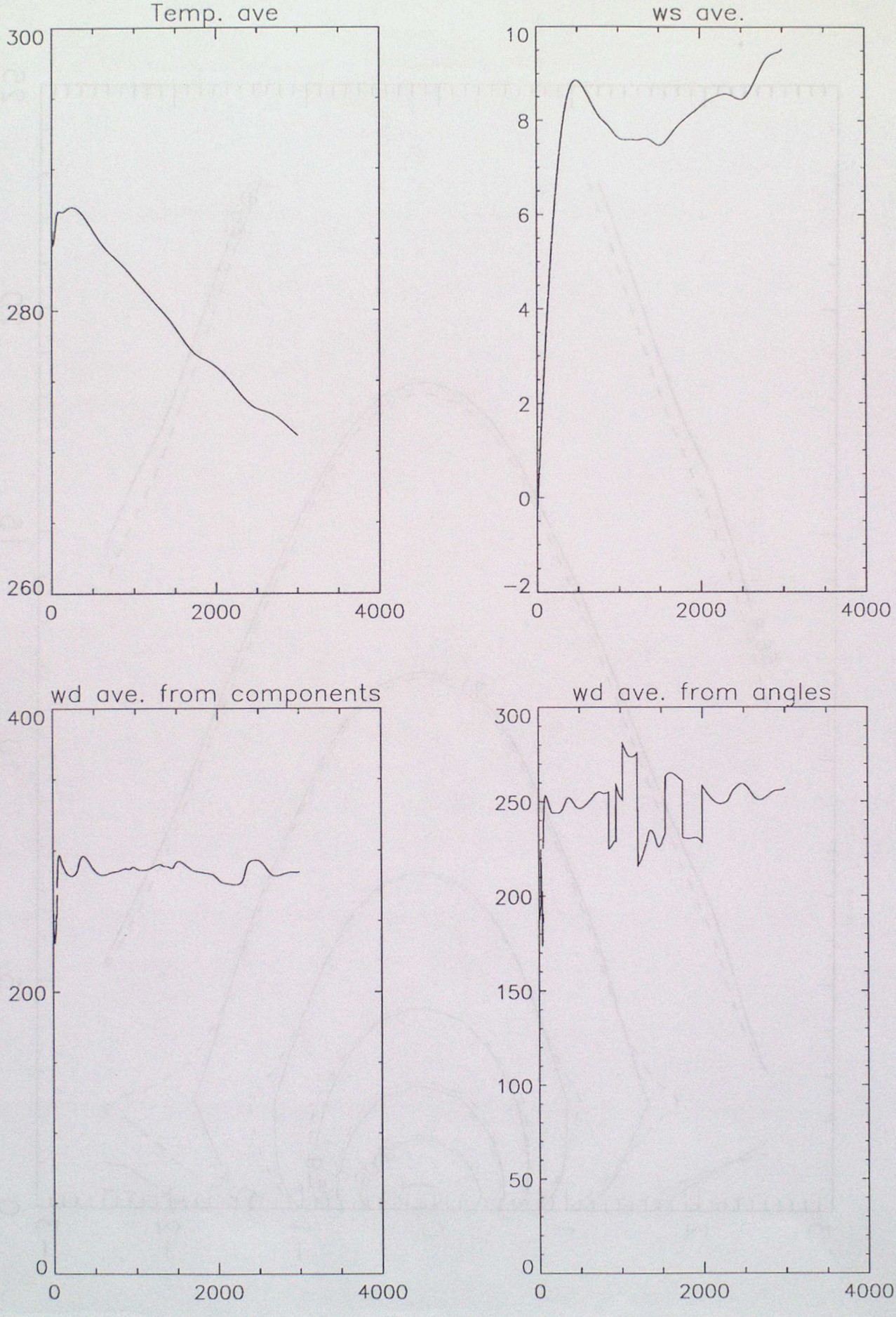

Figure 8a. Meteorological profile for averaged Summer nighttime

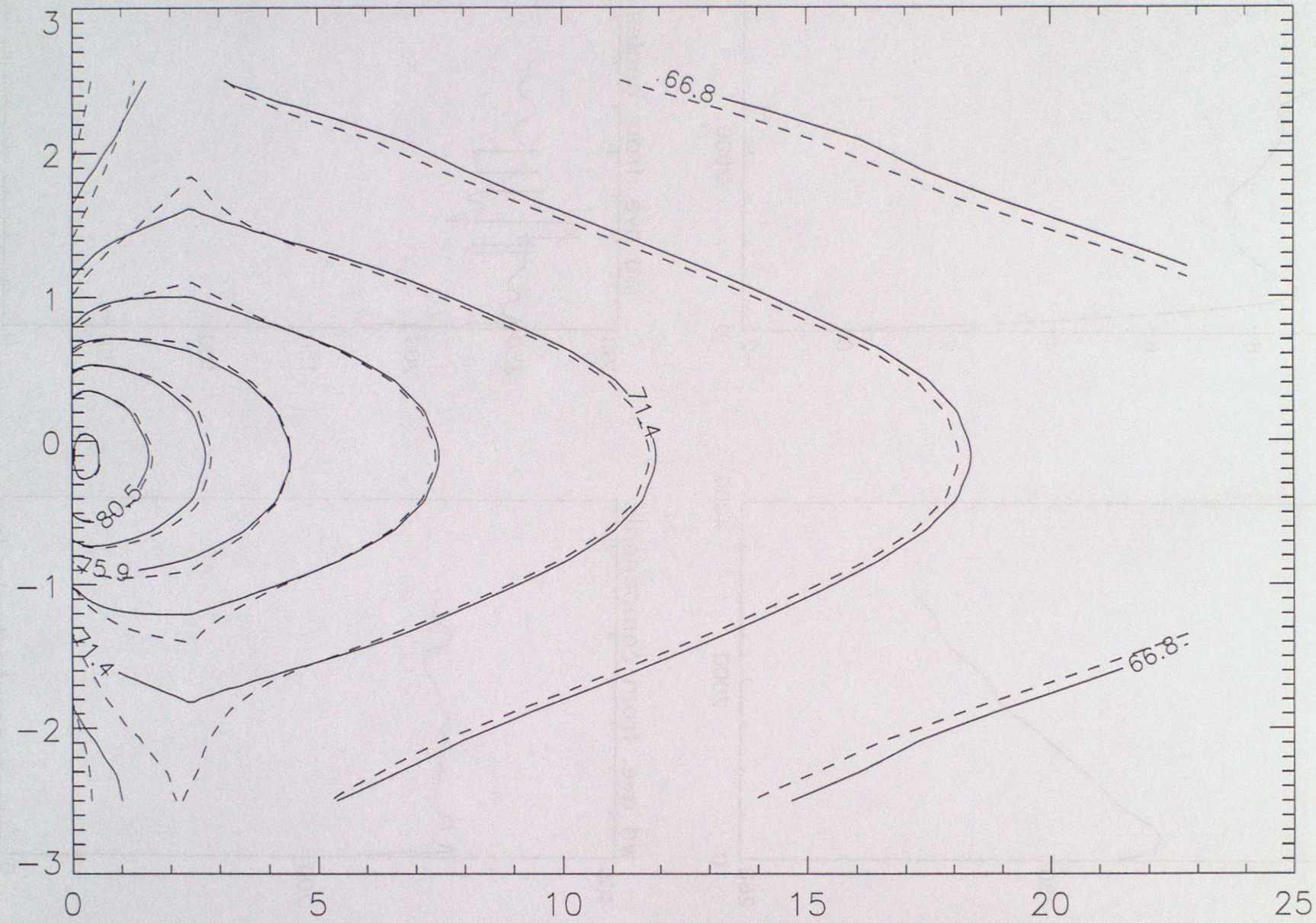

Figure 8b. Noise exposure contours for averaged Summer nighttime

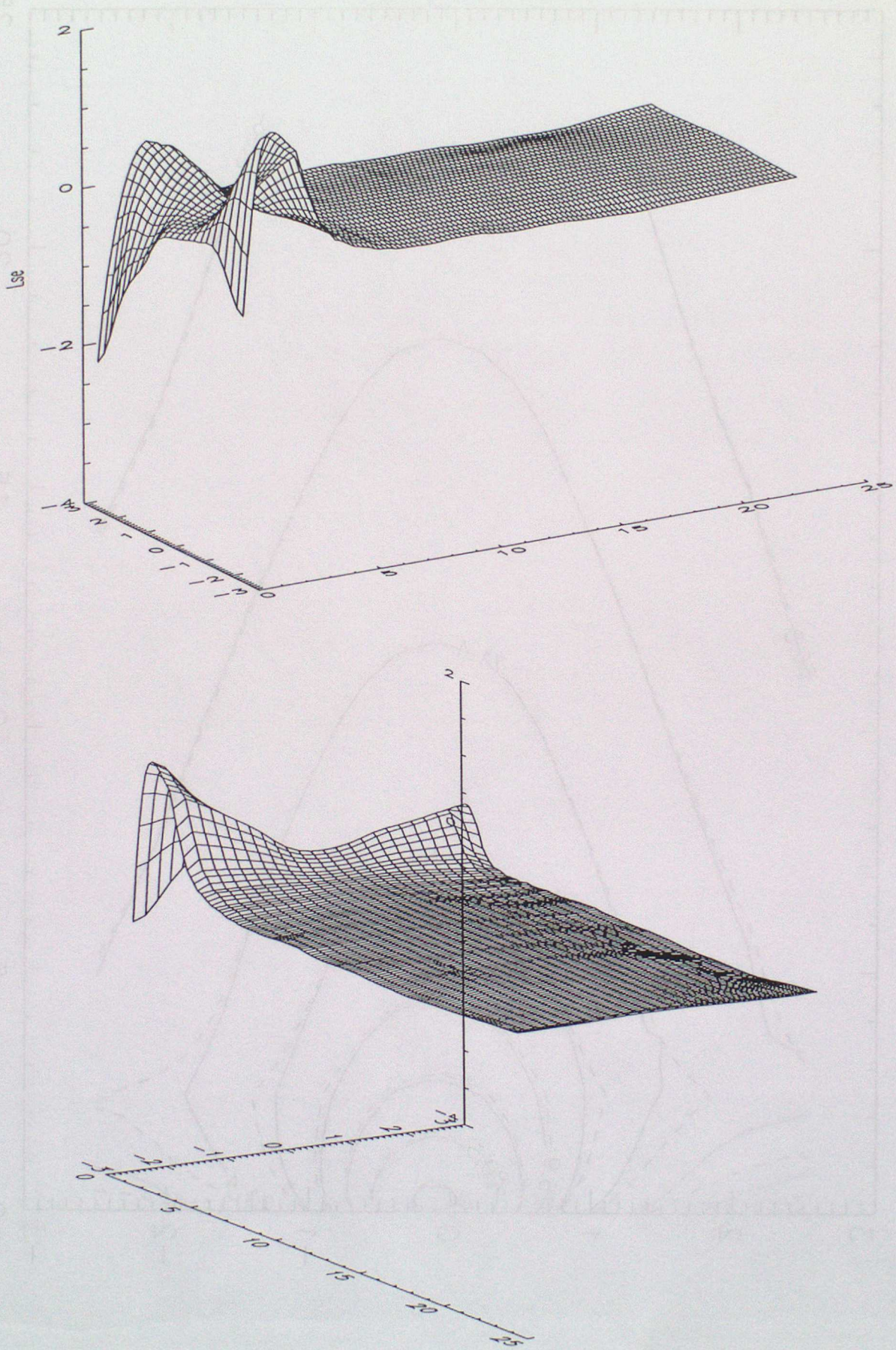

Figure 8c. Surface plot of ΔL_{se} values for averaged Summer nighttime

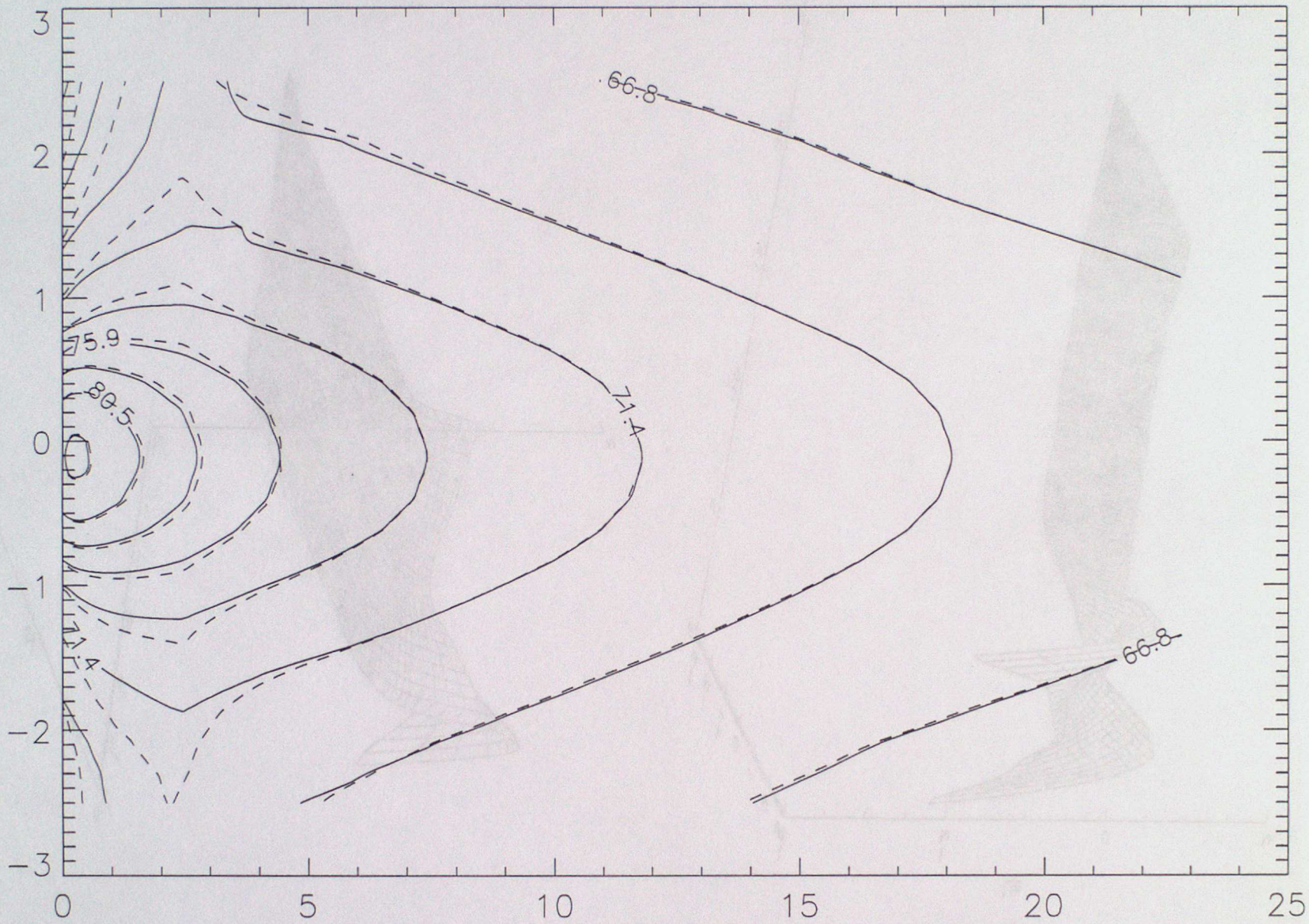

Figure 9a. Noise exposure contours for Summer daytime and nighttime

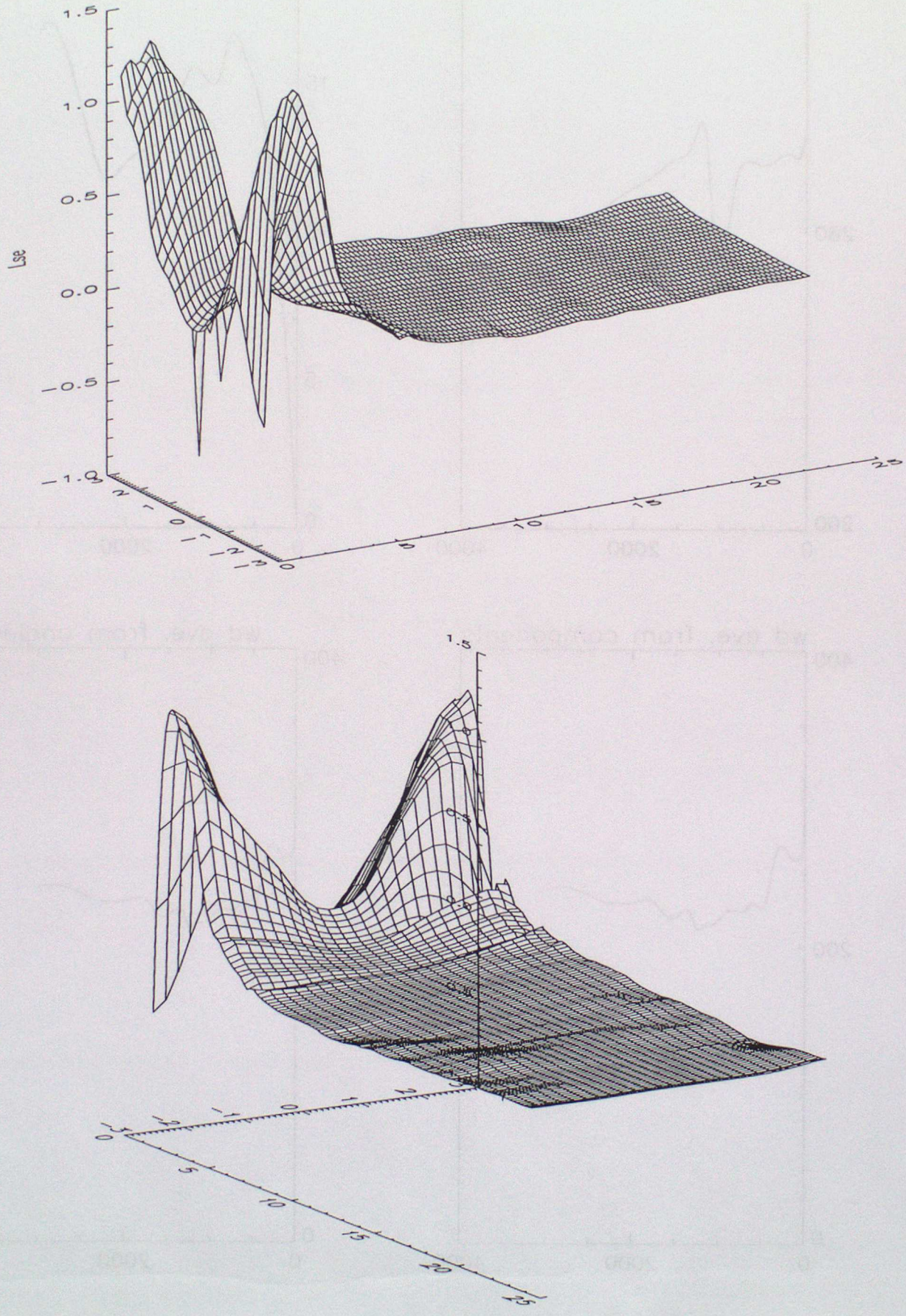

Figure 9b. Surface plot of ΔL_{se} values for Summer daytime and nighttime

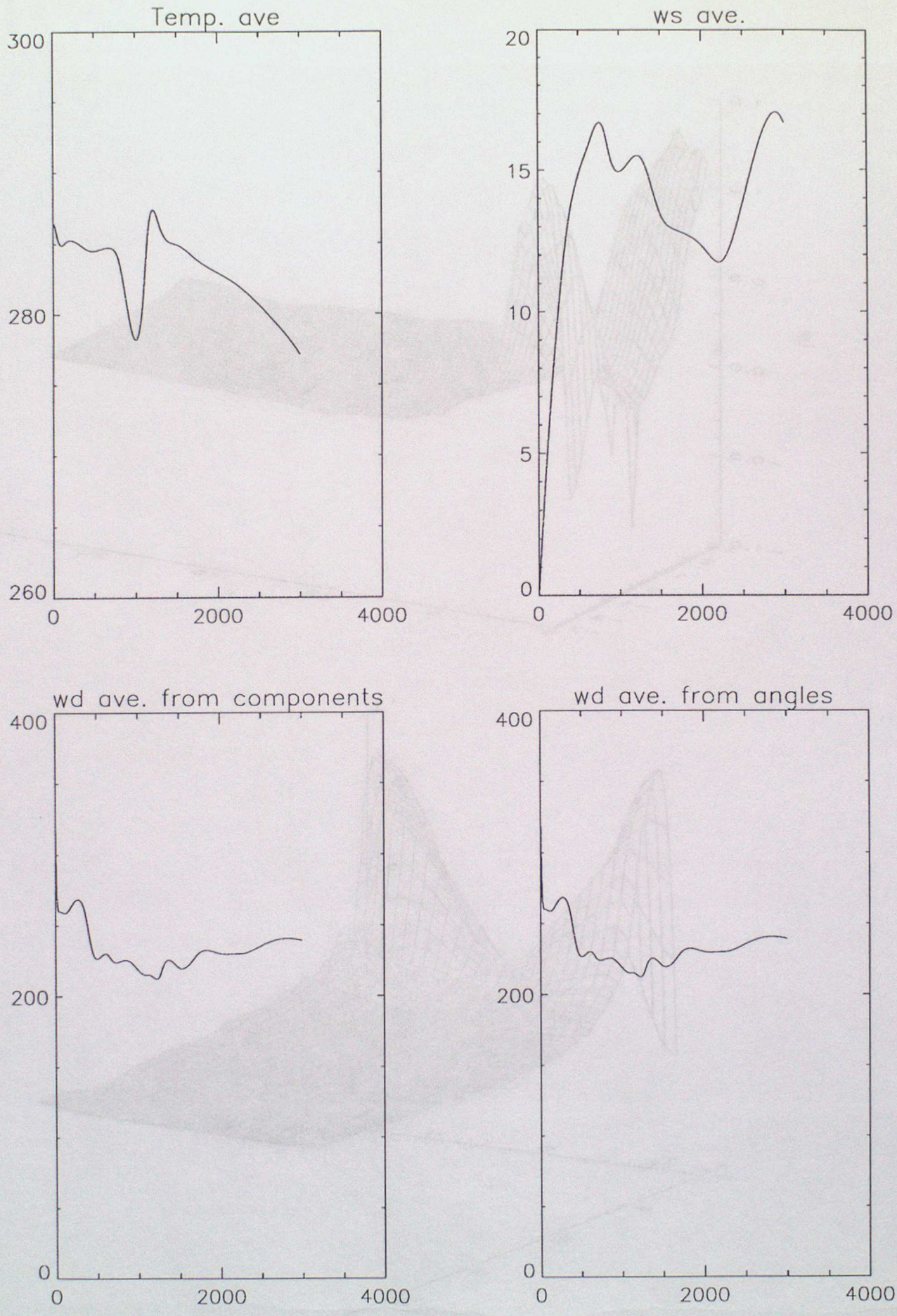

Figure 10a. Meteorological profile for high level inversion

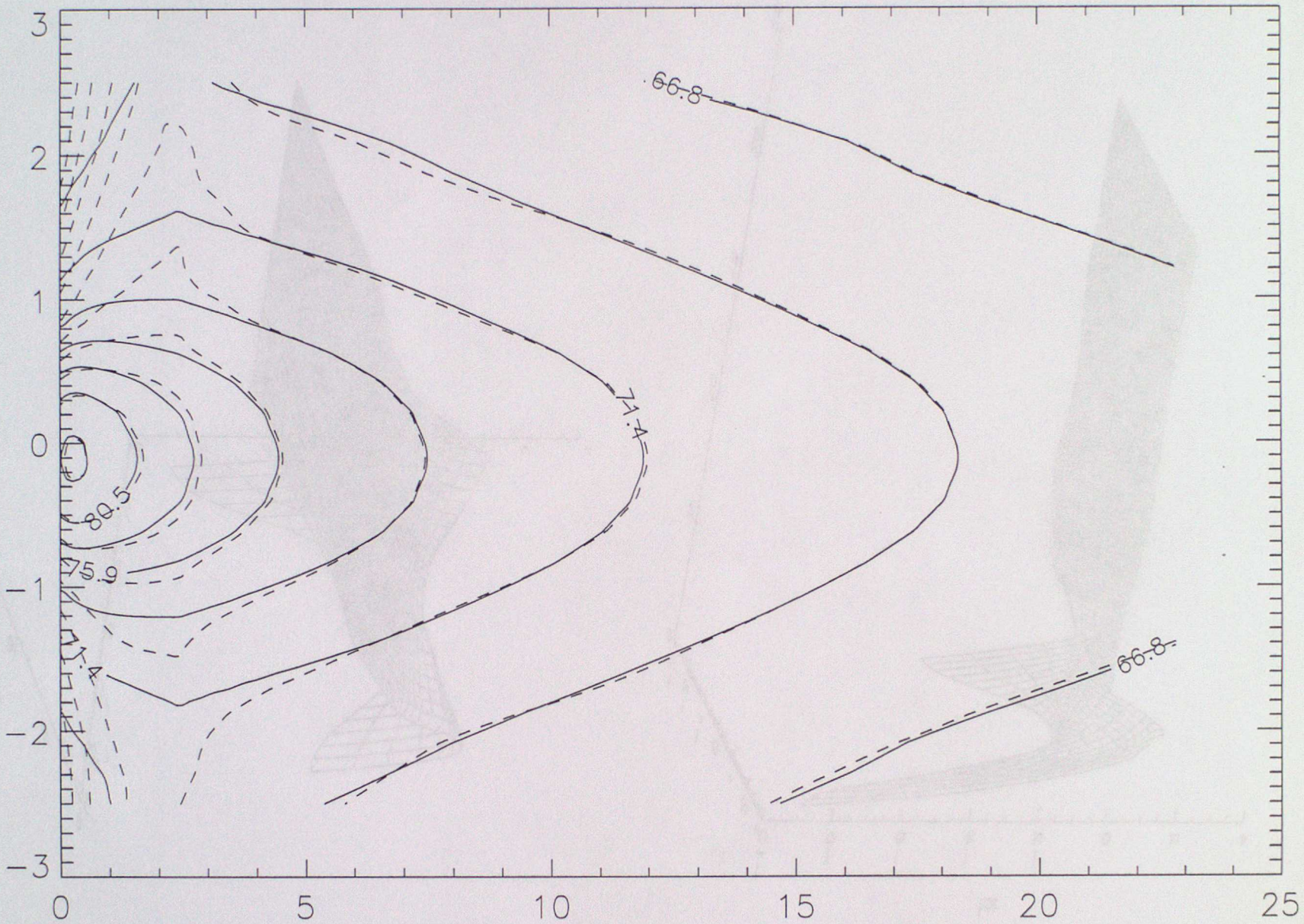

Figure 10b. Noise exposure contours for high level inversion

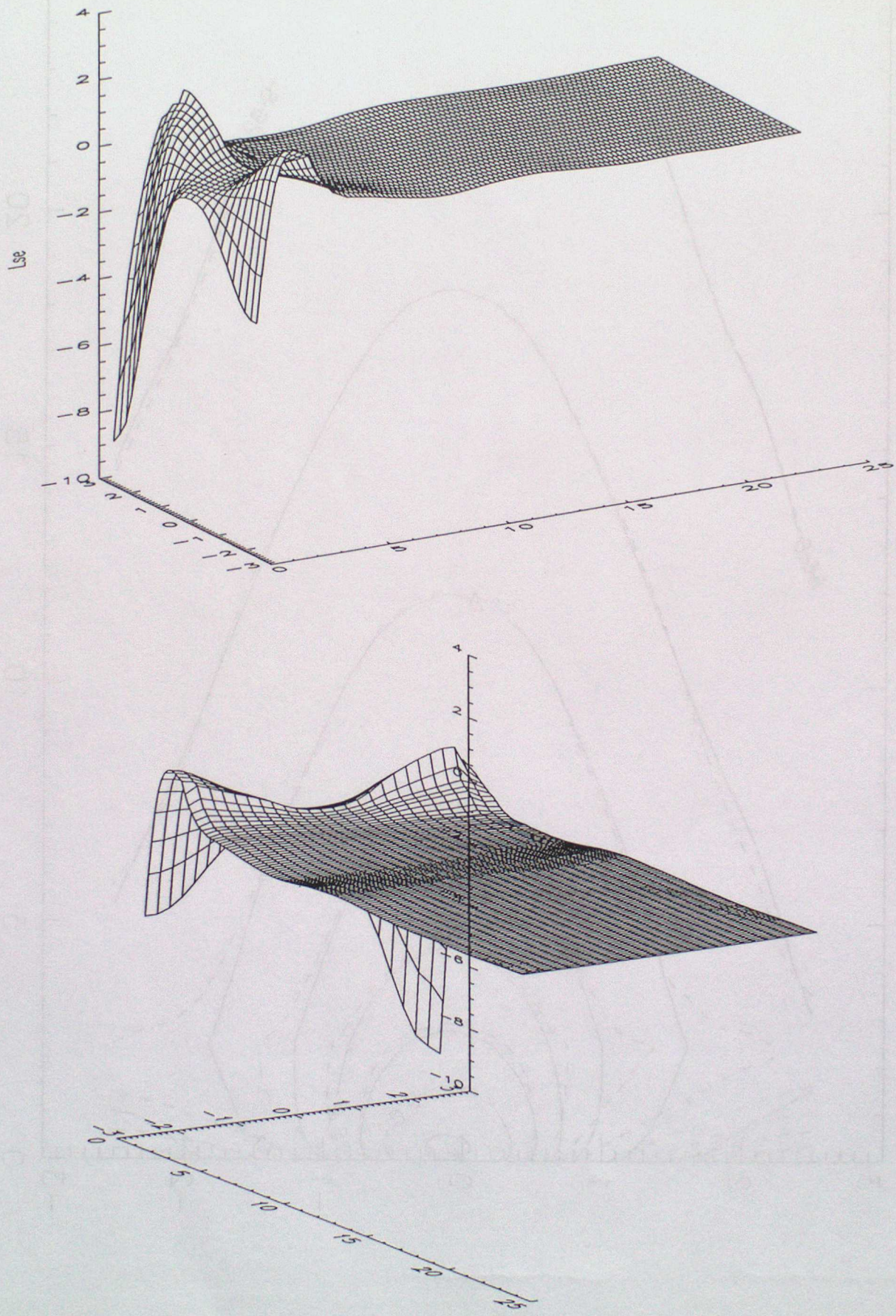

Figure 10c. Surface plot of ΔL_{se} values for high level inversion

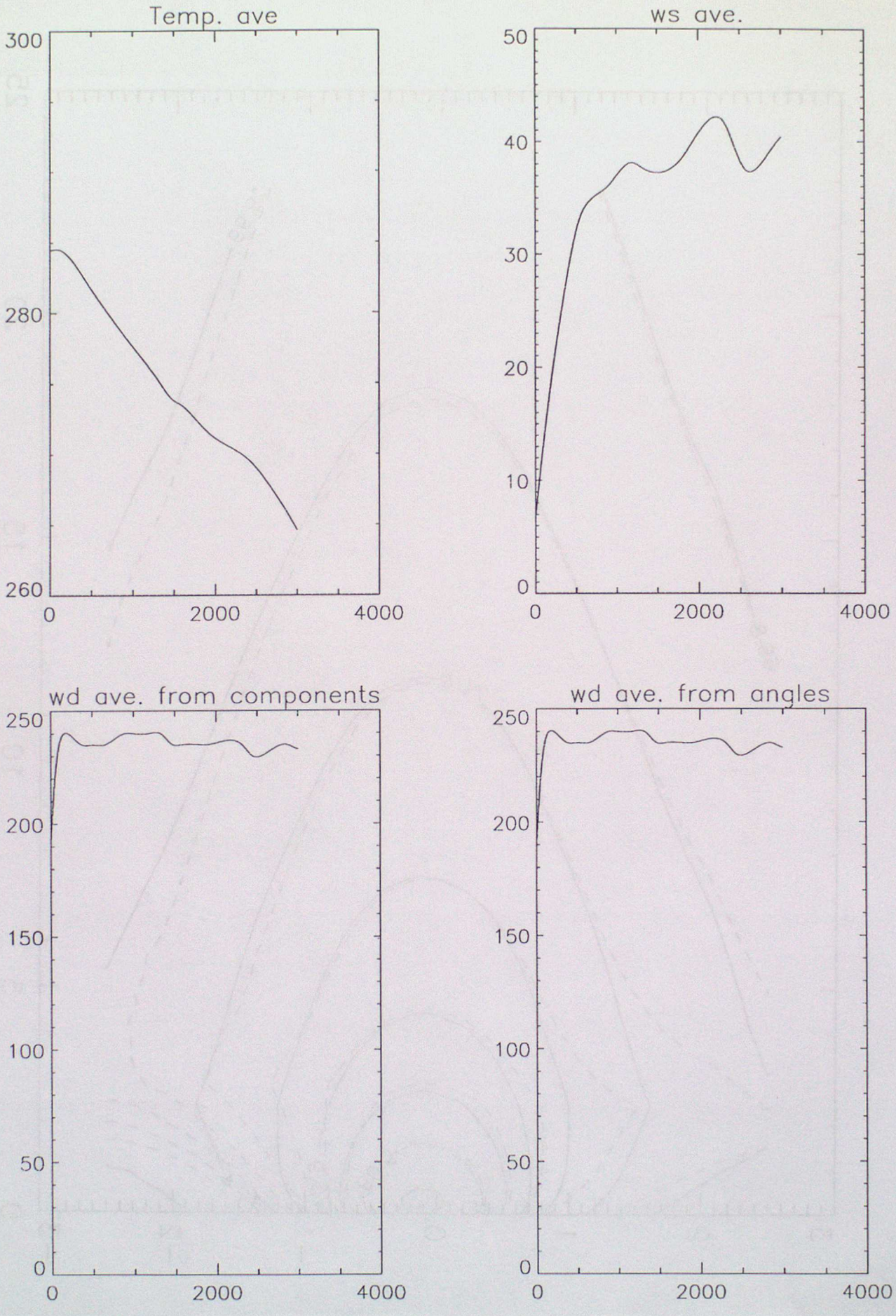

Figure 11a. Meteorological profile for highest wind speed

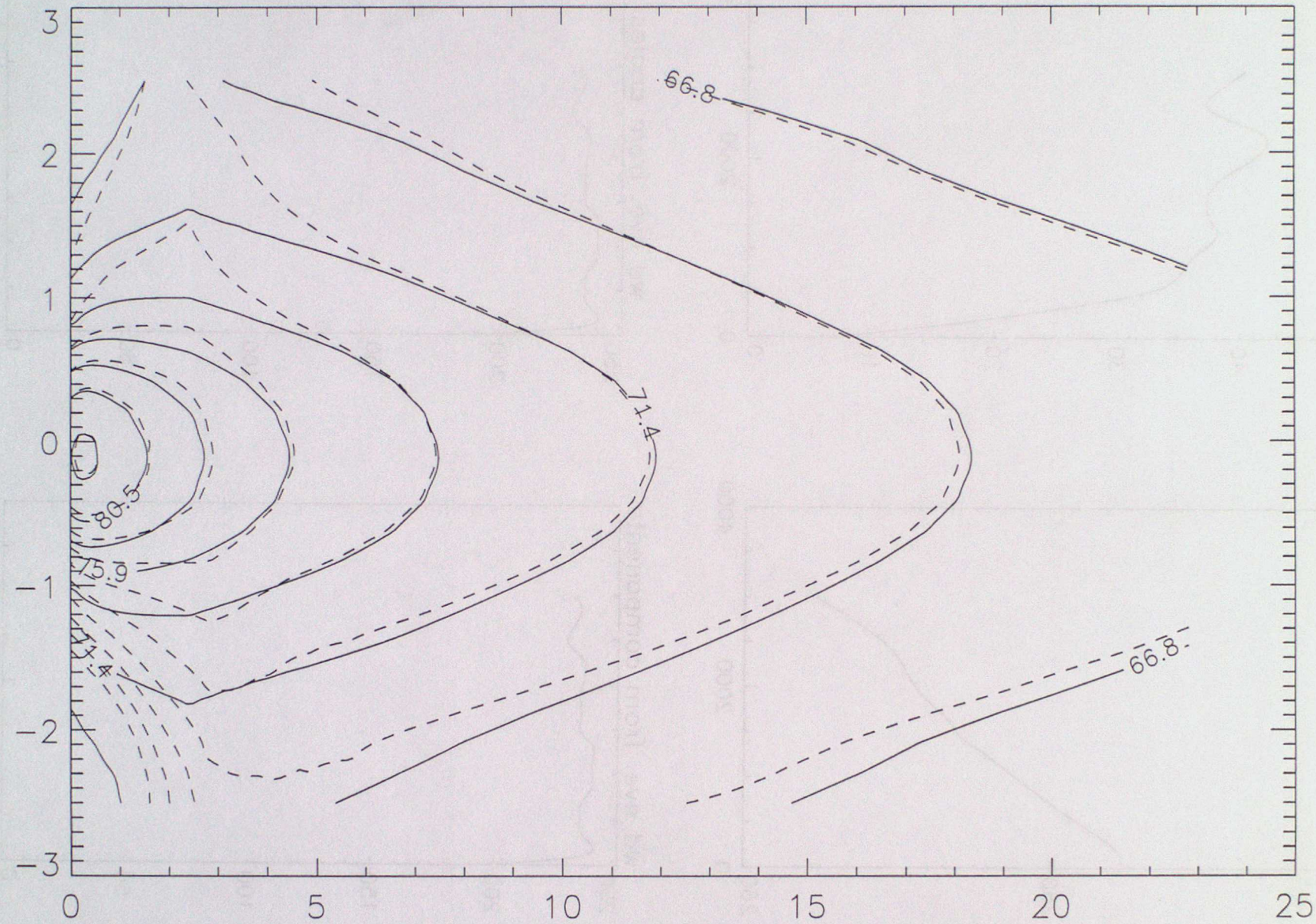

Figure 11b. Noise exposure contours for highest wind speed

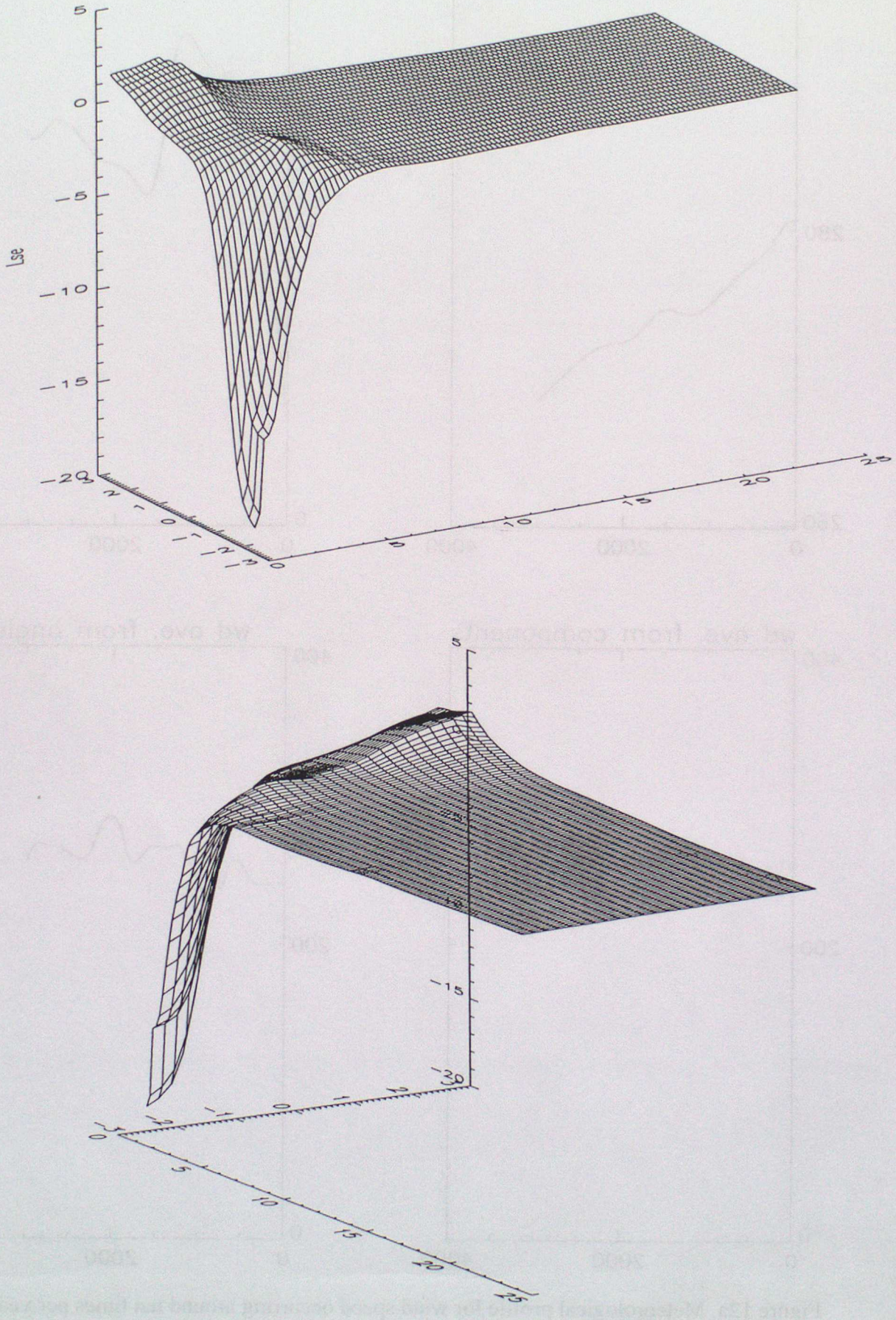

Figure 11c. Surface plot of ΔL_{se} values for highest wind speed

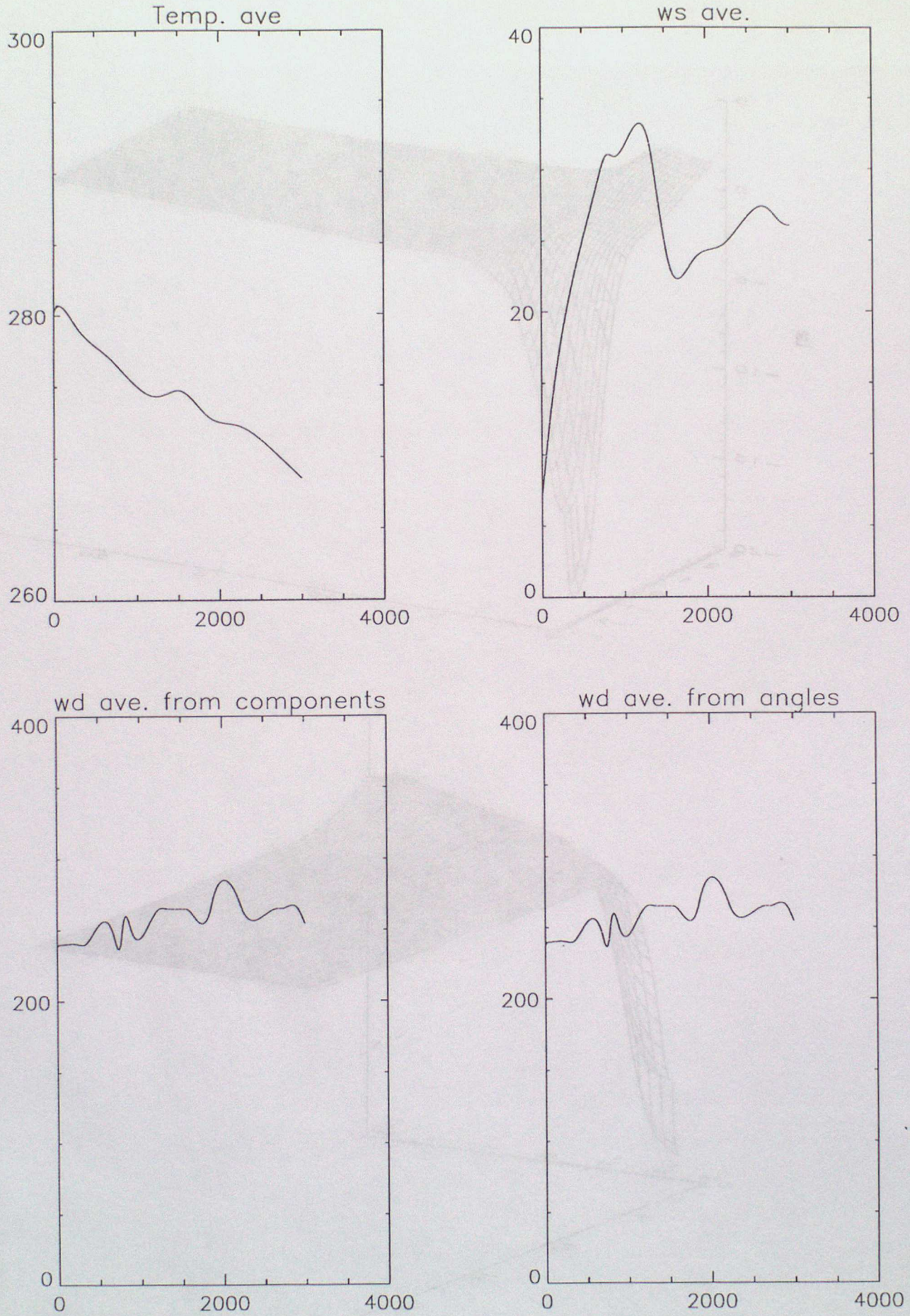

Figure 12a. Meteorological profile for wind speed occurring around ten times per year

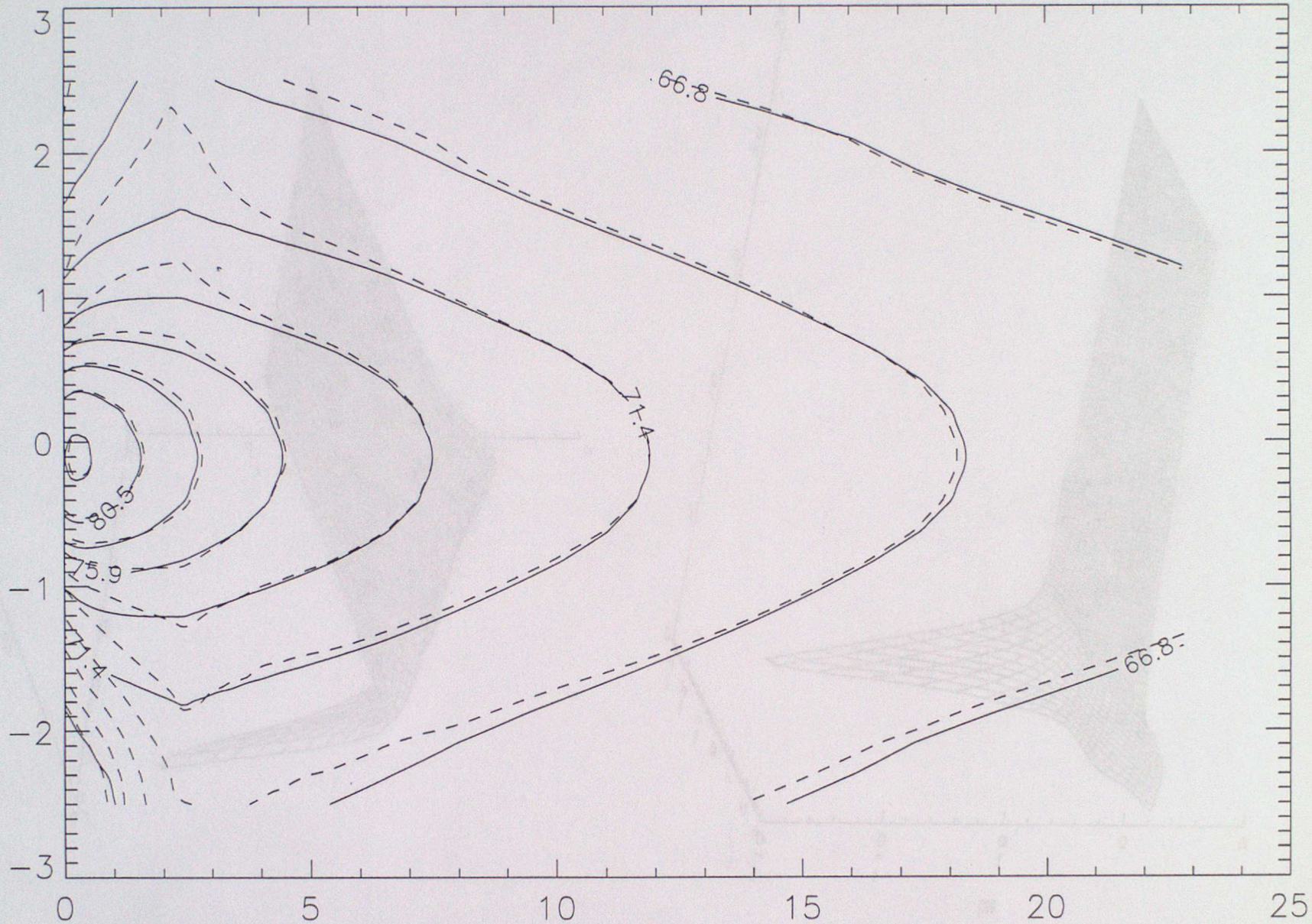

Figure 12b. Noise exposure contours for wind speed occurring around ten times per year

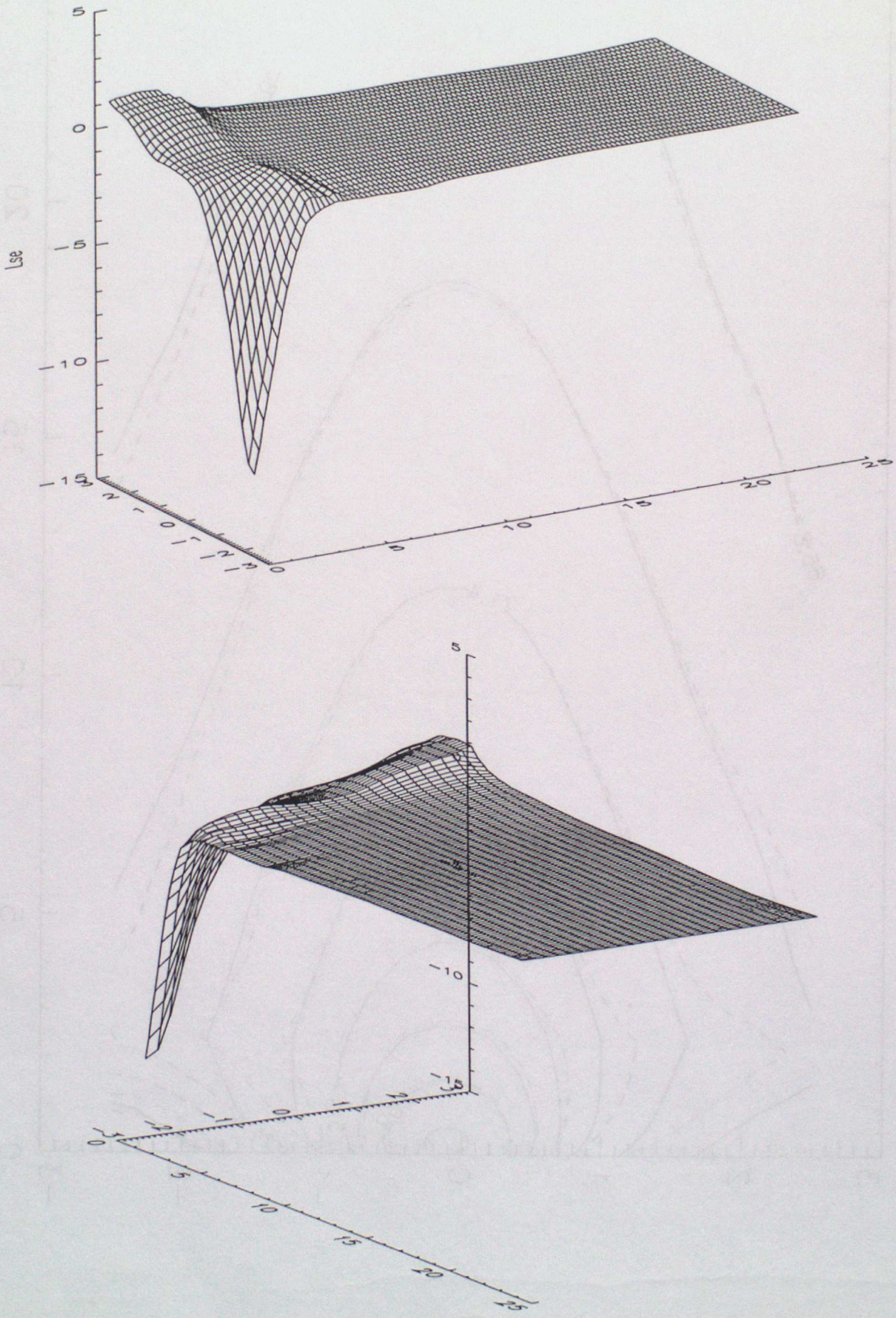

Figure 12c. Surface plot of ΔL_{se} values for wind speed occurring around ten times per year

Appendix 1. Aircraft Ascent Profile

Position and speed data for a number of different aircraft types ascending out of London Heathrow airport were supplied by the CAA [8]. Figure A1 illustrates the profiles actually used in the present noise exposure calculations.

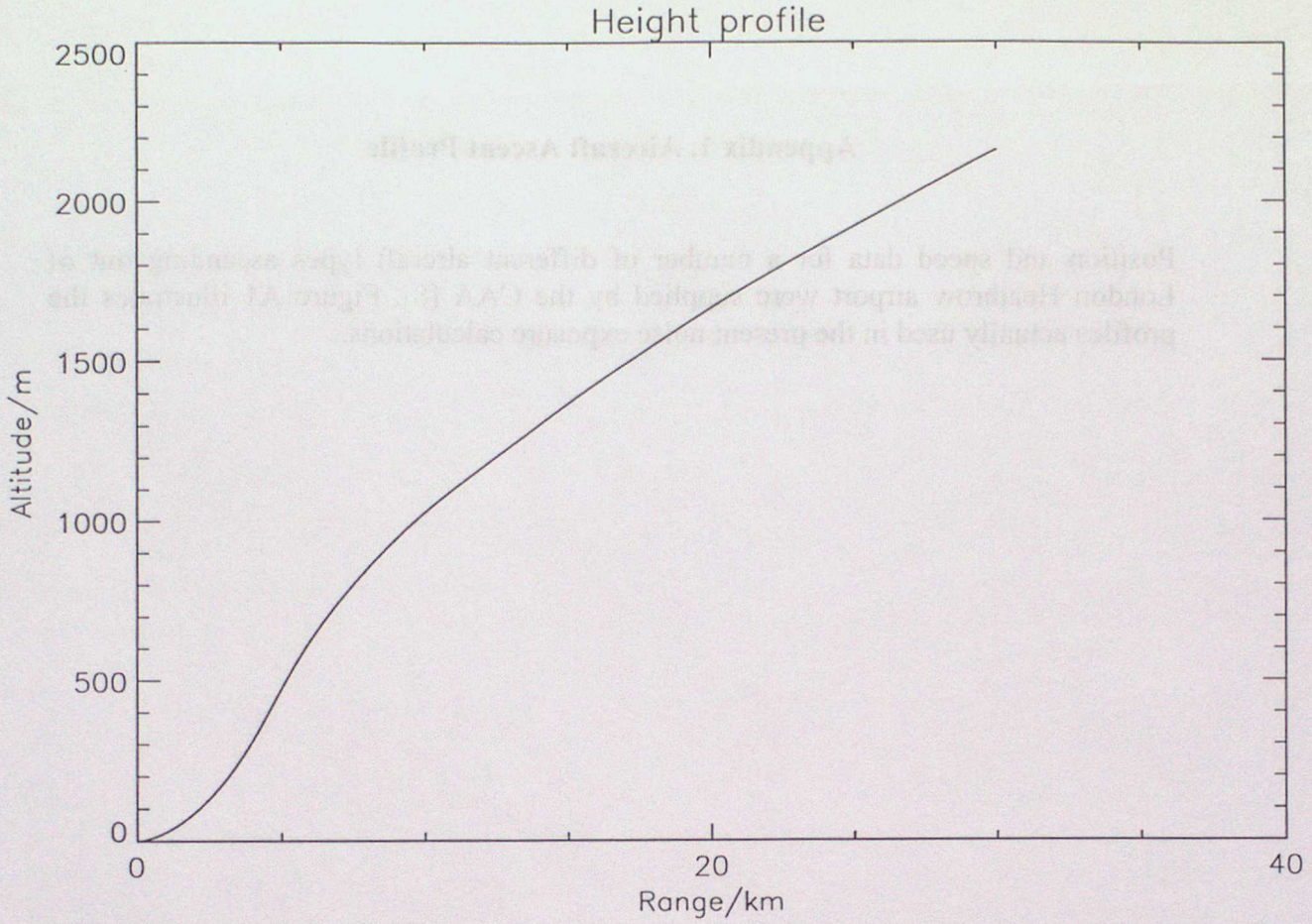

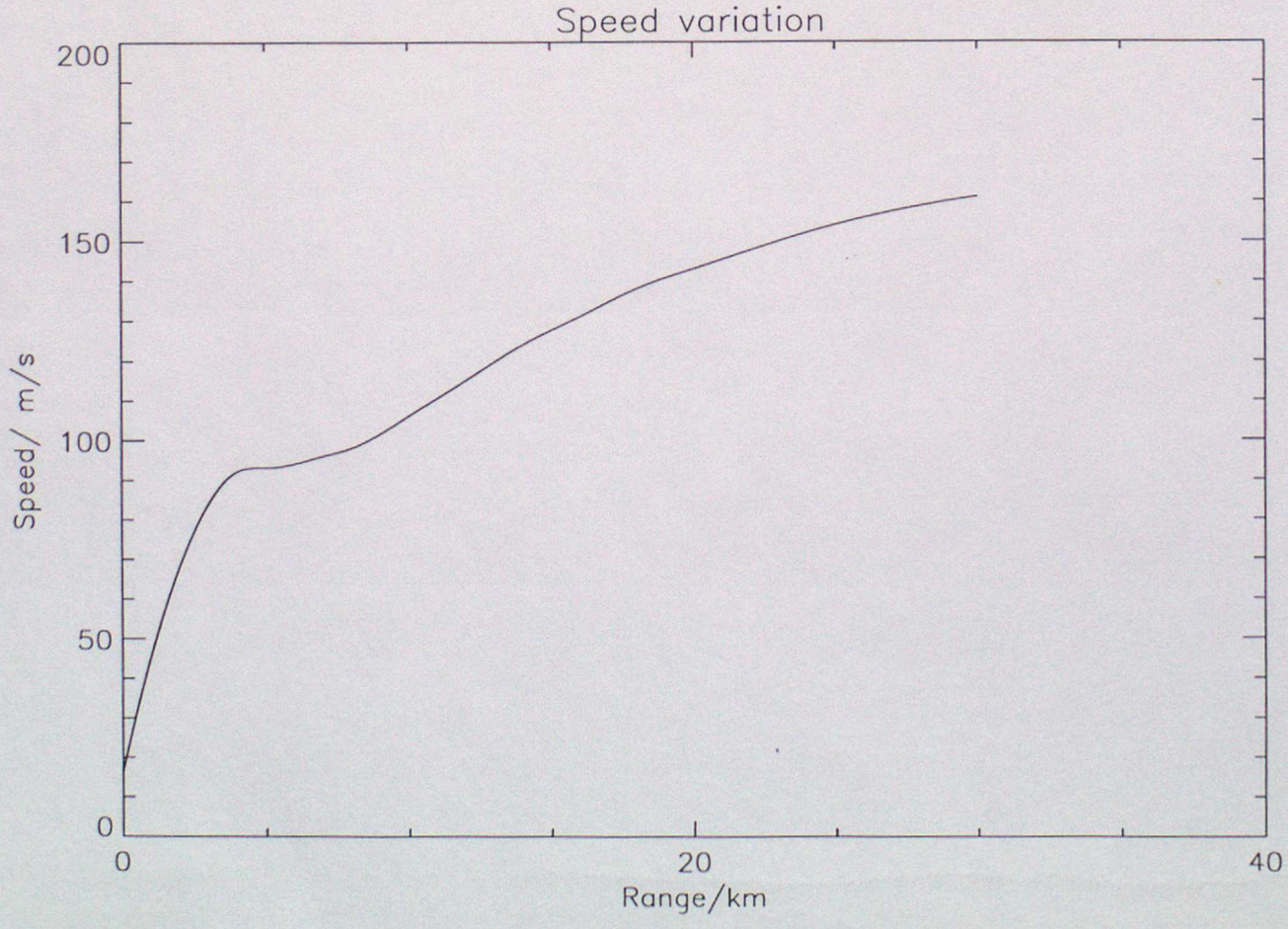

Figure A1. Height and speed variation used in noise calculations [8].

Appendix 2. Seasonally Averaged Meteorological Profiles

Here we present the seasonally averaged meteorological profiles of wind speed, wind direction, and temperature with height up to 3000m. These figures cannot be taken as an accurate climatology since the period over which the averaging was performed is rather short (14 days). However they are sufficient to illustrate the significant seasonal trends. Figures A2a,b,c,d are the profiles for daytime (11am) ascents and Figures A3a,b,c,d are those for nighttime (11pm) ascents.

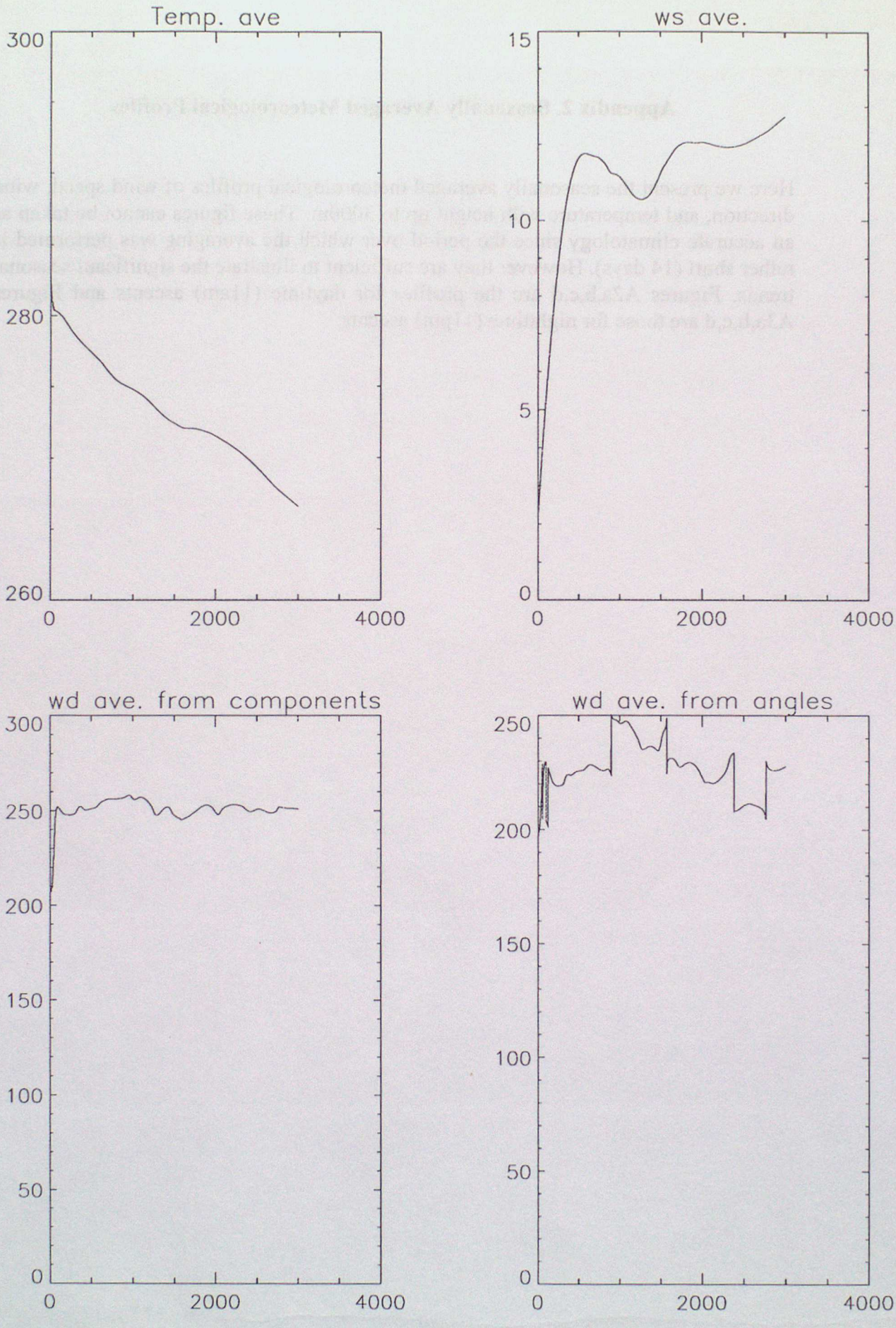

Figure A2a. Seasonally averaged meteorology for Winter daytime

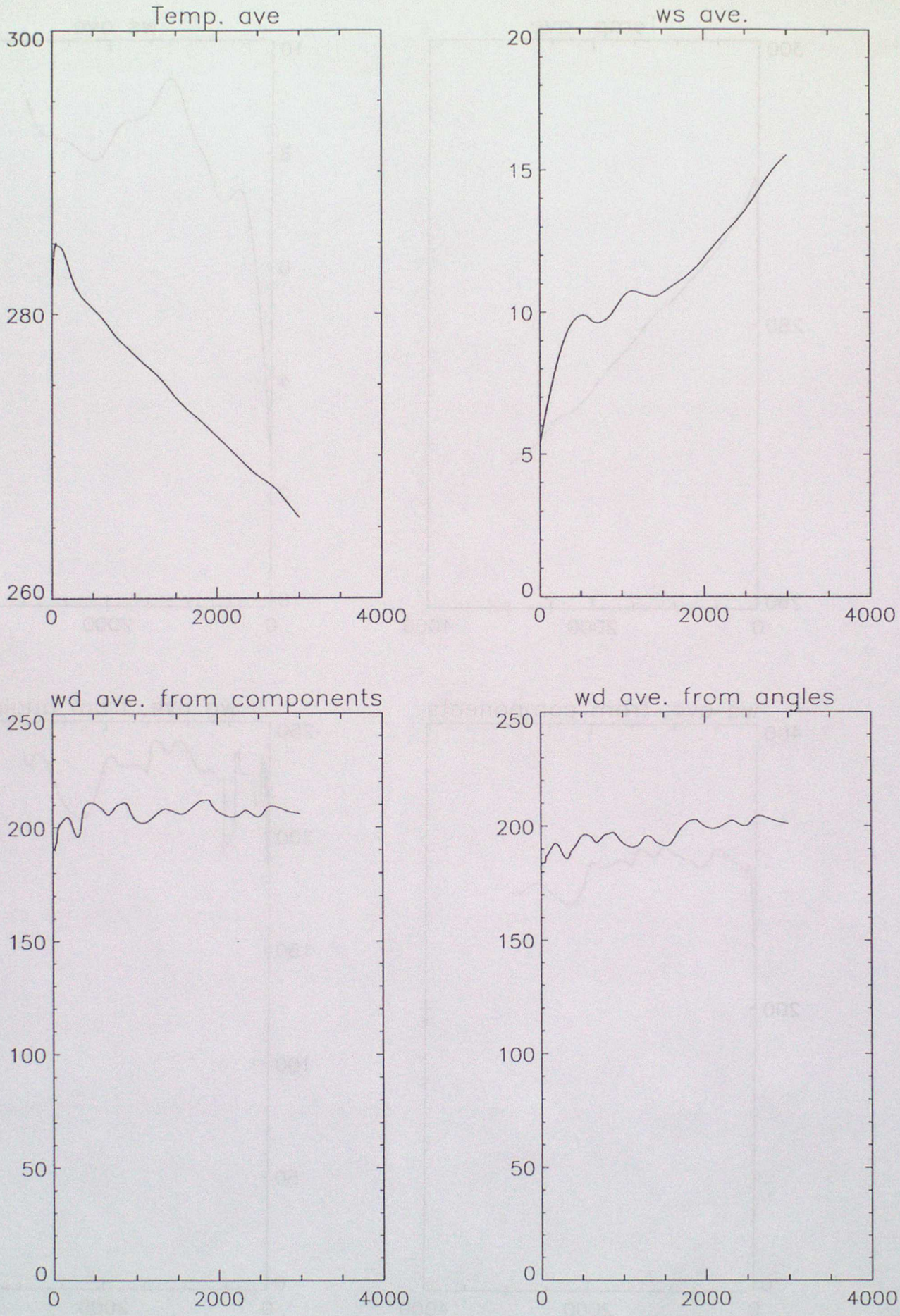

Figure A2b. Seasonally averaged meteorology for Spring daytime

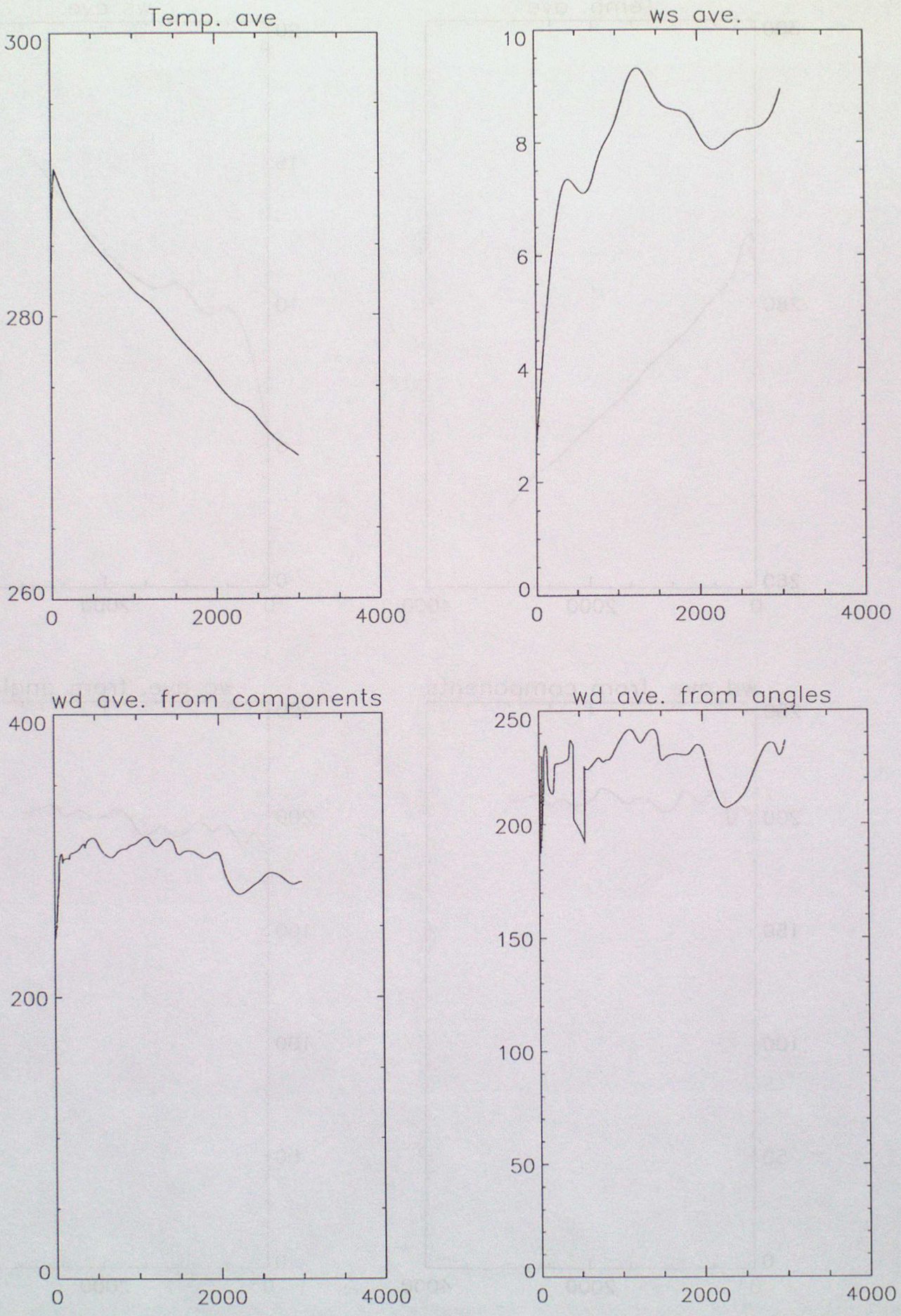

Figure A2c. Seasonally averaged meteorology for Summer daytime

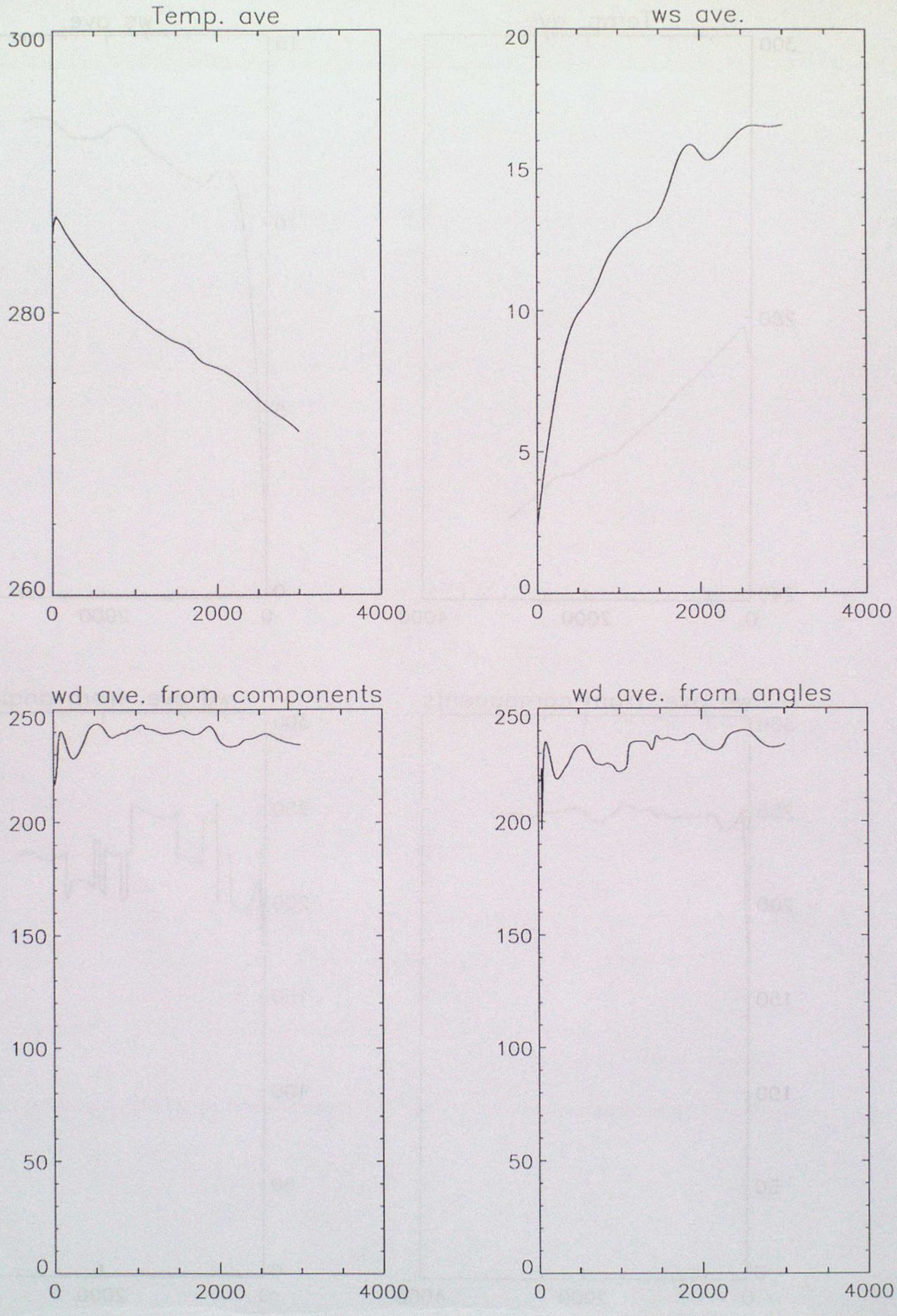

Figure A2d. Seasonally averaged meteorology for Autumn daytime

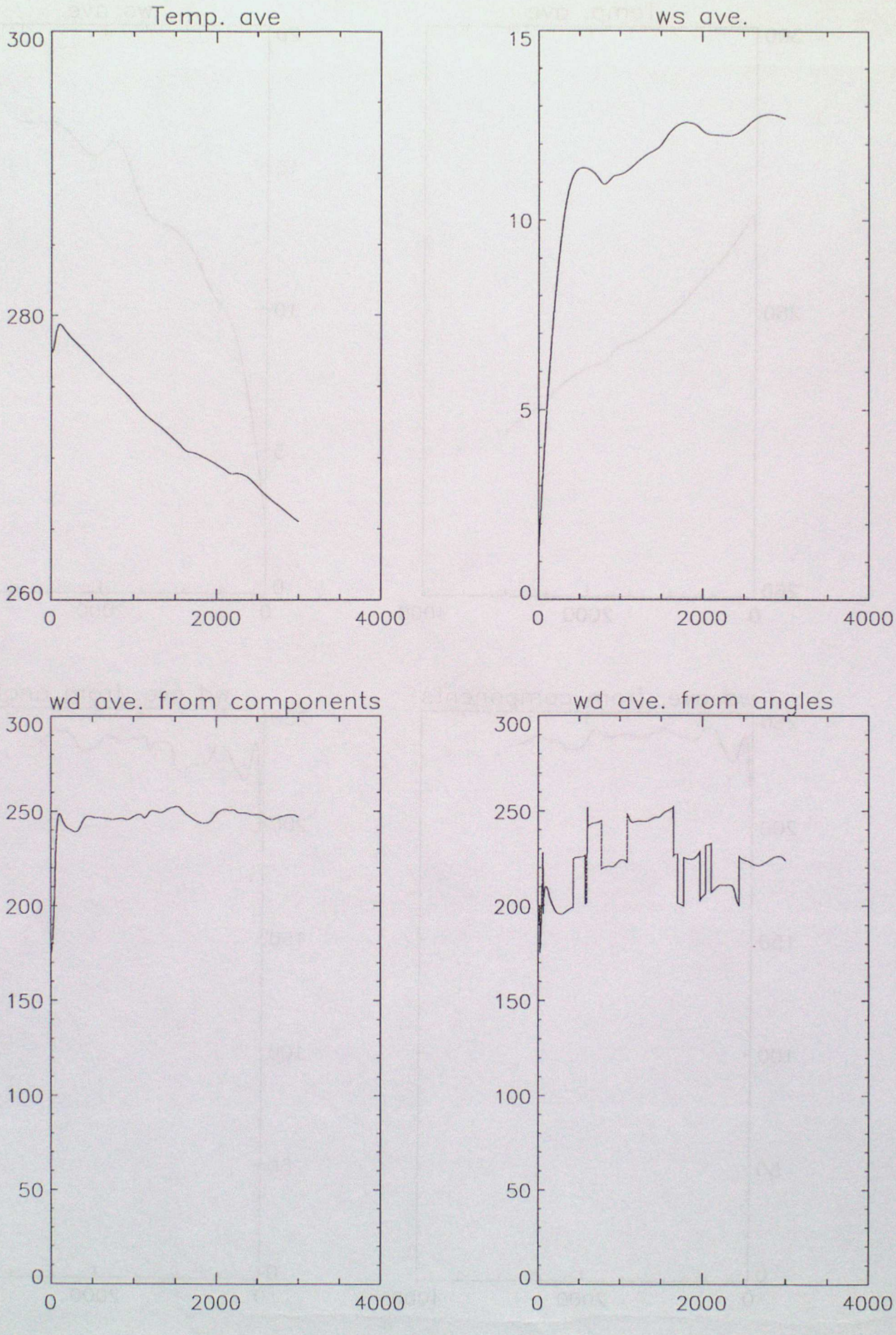

Figure A3a. Seasonally averaged meteorology for Winter nightime

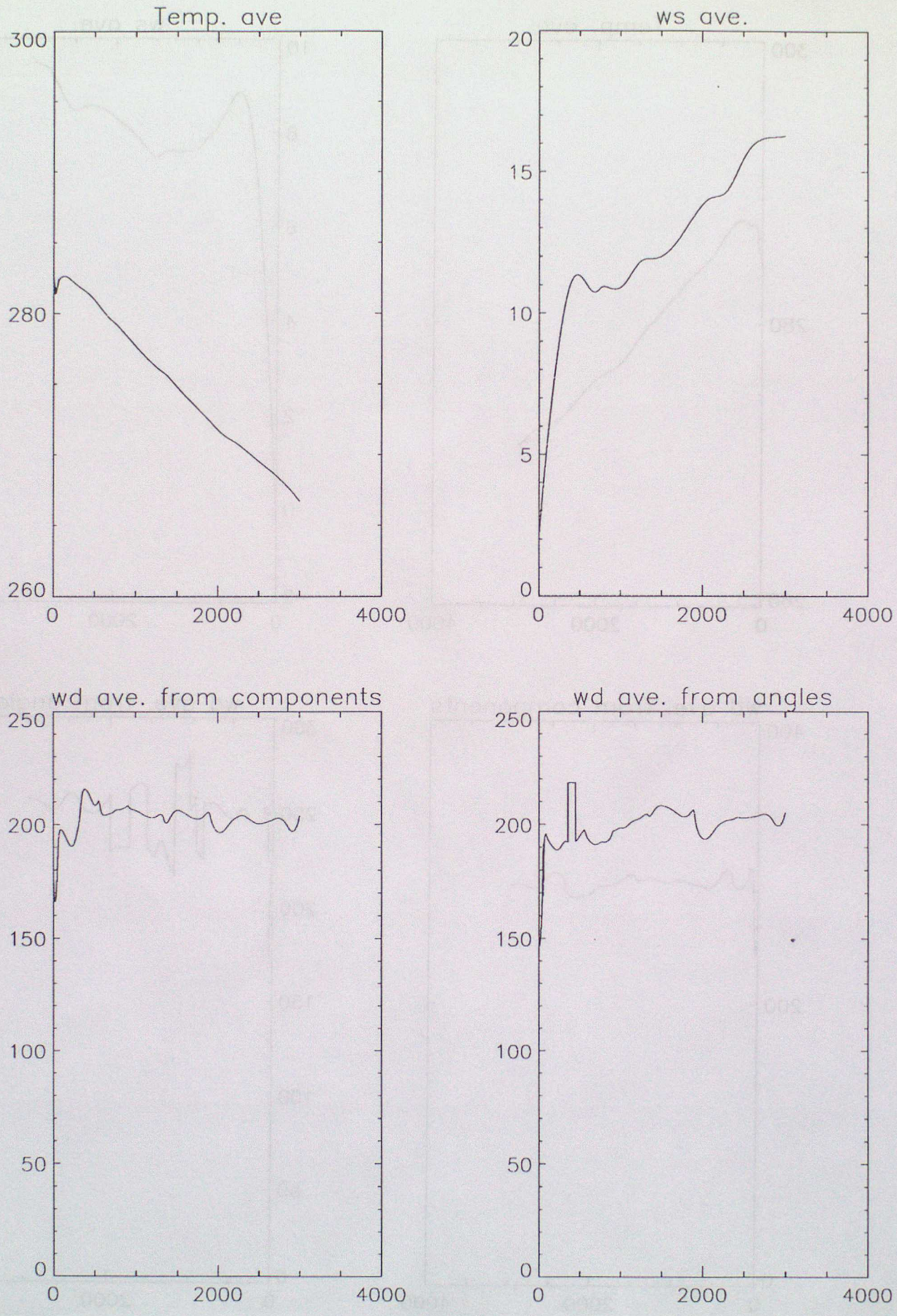

Figure A3b. Seasonally averaged meteorology for Spring nightime

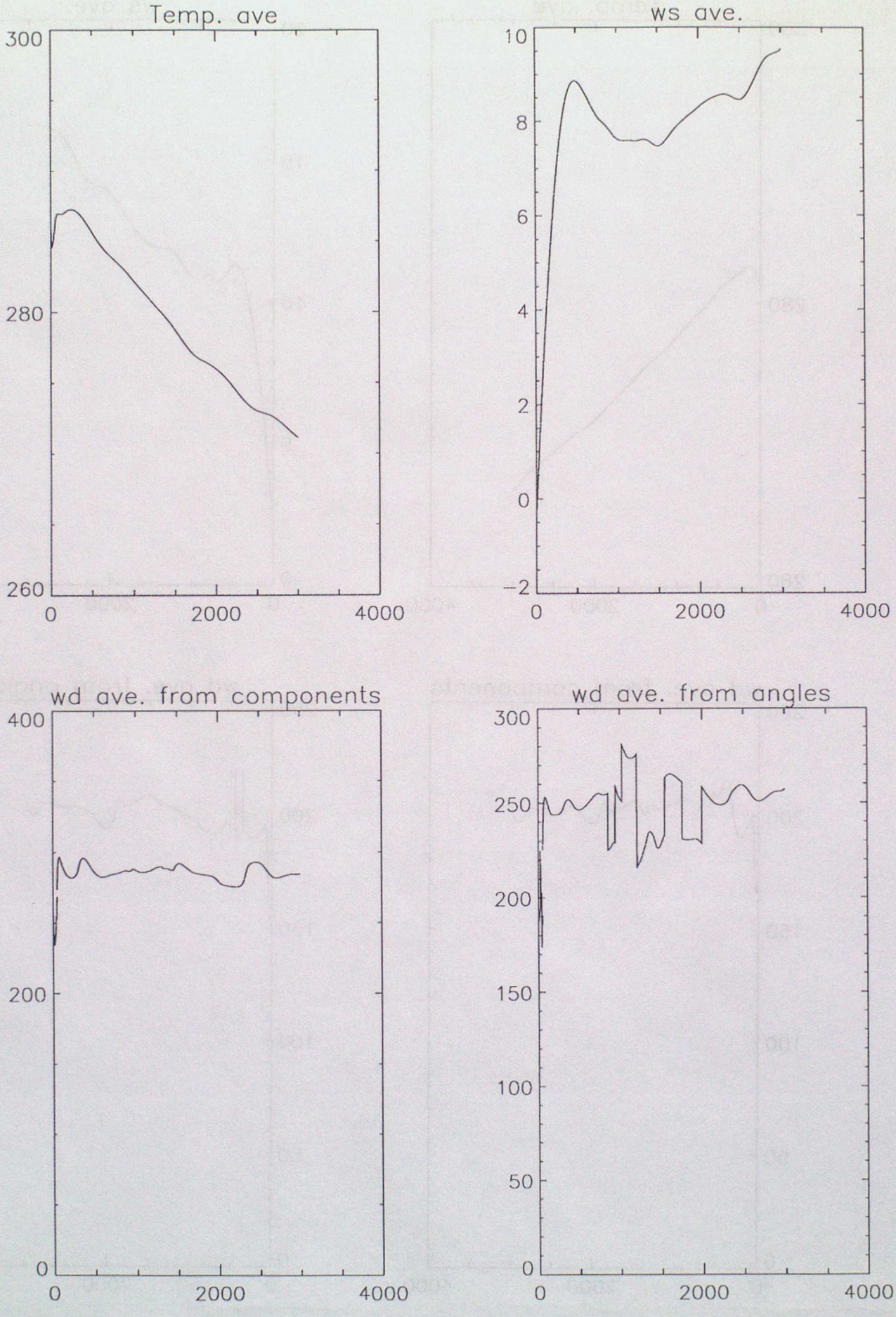

Figure A3c. Seasonally averaged meteorology for Summer nightime

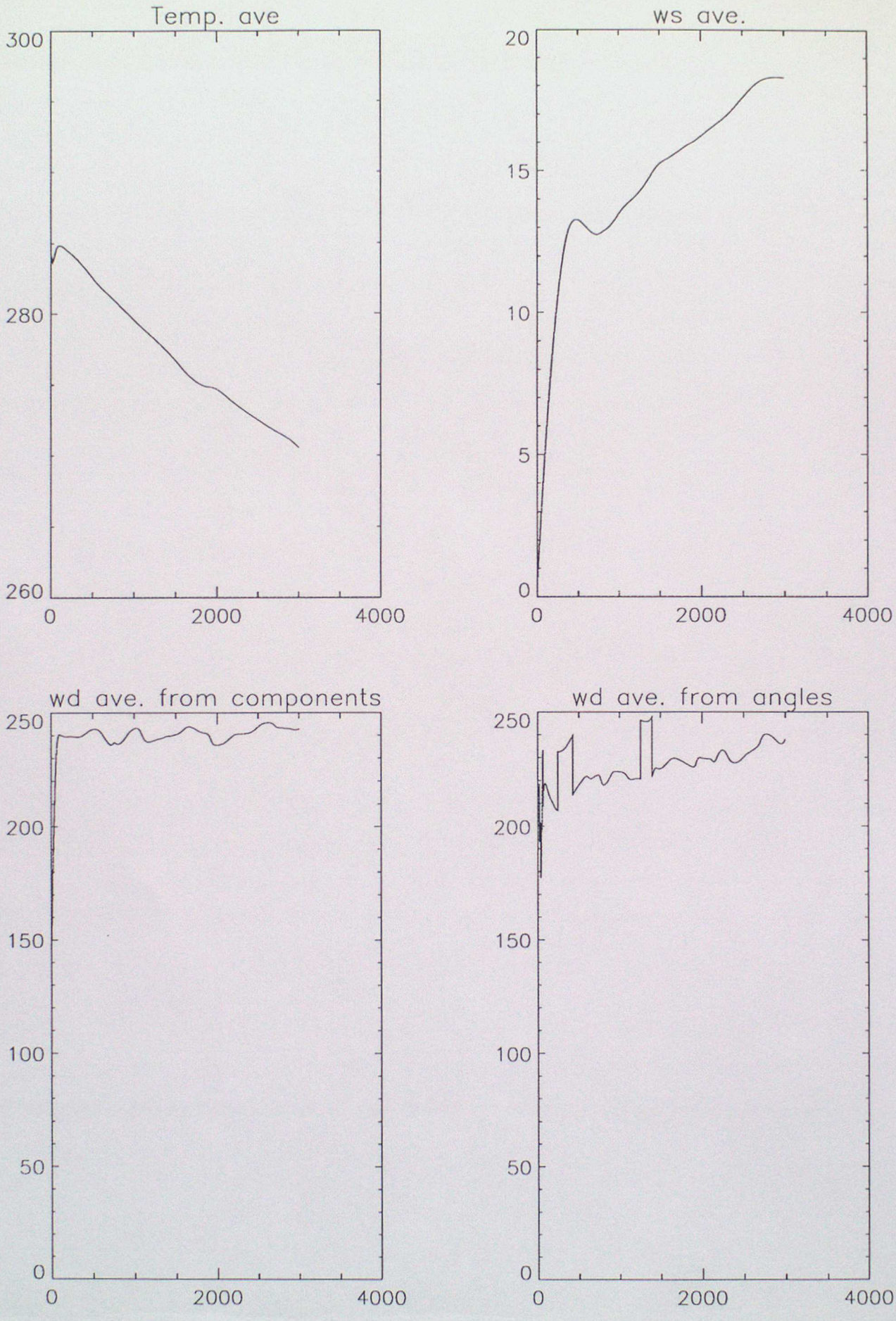

Figure A3d. Seasonally averaged meteorology for Autumn nightime